Partie 4 :

De la vulnérabilité des piétons aux nécessaires évolutions des critères de blessure

Fiche de synthèse

Contributeurs :

Chapitre 1 : Evolution des critères de blessure de la jambe
Ifsttar-LBA

Chapitre 2 : Incidence du design de la face avant du véhicule sur la vulnérabilité du membre pelvien *Ifsttar-LBA / Polytechnico Turin*

Chapitre 3 : Evolution des critères de blessure de la tête
UDS

Questions posées

L'analyse des mécanismes de blessure sur le membre pelvien ou encore sur l'extrémité céphalique montre des différences significatives qui au-delà de la variabilité des situations d'impact doivent tenir compte de la diversité du parc automobile et des conditions de choc. L'analyse détaillée offerte par les outils de simulation par éléments finis montre enfin que les processus de blessure ne sont pas uniques et naissent de la combinaison de plusieurs mécanismes.

Les questions posées dans cette partie portent sur la prise en compte de la variabilité du parc automobile et de manière conjuguée les évolutions nécessaires à proposer concernant les critères de blessure de l'extrémité céphalique et du membre pelvien.

Chapitre 1 : Evolutions des critères de blessure de la jambe

Ce chapitre pose les bases d'évolutions significatives des critères de blessure existants du membre pelvien. Il traite de manière disjointe le risque de blessure osseuse du risque d'atteinte du genou ligamentaire. Enfin, les critères de blessure proposés sont établis à la fois sur la base de cas d'impact dits académiques que sur des situations réalistes d'impact piétons. Les résultats de ce travail sont présentés sous forme d'articles.

I. Injury tolerance of tibia for the car–pedestrian impact

This article is published in the journal- Accident Analysis and Prevention:
Mo F, Arnoux PJ, Jure JJ, Masson C. Injury tolerance of tibia for the car–pedestrian impact. Accident Analysis & Prevention. 2012; 46(0):18-25.
This work aims to investigate the injury tolerance of tibia fracture with combined experimental data and numerical simulations. Eleven new reported quasi-static bending tests of tibia mid-shaft, and additional eleven dynamic mid-shaft bending test results in the previous literature were used to define injury risk functions. Furthermore, to investigate the influence of tibia locations on bending tolerances, finite element simulations with lower limb model were implemented according to three-point bending and pedestrian impact conditions.
Résultats marquants : Tibia injury criteria (depending of impact location).
The regressive curve of the tibia bending tolerance was obtained from the simulations on the different impact locations, and indicated that the tibia fracture tolerance could vary largely due to the impact locations for the car-pedestrian crash.

II. Coupling Lateral Bending and Shearing Mechanisms to Define Knee Injury Criteria for Pedestrian Safety

This article is published in Traffic Injury Prevention Journal : Fuhao M, Masson C., Arnoux PJ., Coupling Lateral Bending and Shearing Mechanisms to Define Knee Injury Criteria for Pedestrian Safety, (2013) 14, 378–386
Objective: Regarding the combined lateral bending and shearing contributions of knee joint kinematics, developing a coupled knee injury criterion is necessary for improving vehicle countermeasures to mitigate pedestrian knee injuries.
Methods: First, 7 isolated lower limb tests from postmortem human subjects (PMHS) were reported, with dynamic loading at a velocity of 20 km/h. With the intention of replicating relevant injury mechanisms of vehicle–pedestrian impacts, the experimental tests were categorized into 3 groups by the impact locations on the tibia: the distal end to prioritize pure bending, the middle diaphysis to have combined bending and shearing effects, and the proximal end to acquire pure shearing. Then, the corresponding FE model was employed to provide an additional way to determine exact injury occurrences and develop a robust knee injury criterion by the variation in both the lateral bending and shearing contributions through a sensitivity analysis of impact locations.
Résultats marquants : Knee joint injury criteria (combining shearing and bending) and validated with sub-segment tests
Both the tolerances and patterns of knee joint injuries were determined to be influenced by impact locations due to various combined contributions of lateral bending and shearing. Both medial collateral ligament and cruciate ligament failures were noted as the onsets of knee injuries, namely, initial injuries. Finally, a new injury criterion categorized by initial injury patterns of knee joint was proposed by coupling lateral bending and shearing levels.
Conclusions: The developed injury criterion correlated the combined joint kinematics to initial knee injuries based on subsegment tests and FE simulations conducted with a biofidelic lower limb model. This provides a valuable way of predicting the risk of knee injury associated with vehicle–pedestrian crashes and thereby represents a further step to promote the design of vehicle countermeasures for pedestrian safety.

III. Investigation of the injury threshold of knee ligaments by the parametric study of car-pedestrian impact conditions

This article is published in Safety Science : Mo F, Arnoux PJ, Cesari D, Masson C. Investigation of the injury threshold of knee ligaments by the parametric study of car-pedestrian impact conditions. Safety Science. 62, 2014, 58–67

Since the first European Committee directive for pedestrian safety was published, vehicle suppliers have implemented pedestrian protection requirements to automobile structures at the design level. As to the development of current automobile front-end structures, a question arises about pedestrian safety: are there existing injury criteria for the new generation of cars? Most previous injury thresholds for knee ligaments were principally based on isolated sub-segment tests with contrived loading conditions, and rarely took the entire front-end shape of the car model into account to simulate realistic pedestrian loading conditions.

Hence, the current study aims to investigate injury thresholds of primary knee ligament injuries in car-pedestrian impact environments as well as to evaluate the previous criteria proposed by isolated sub-segment tests. The entire front-end shape of a car model was employed. A parametric study of various pedestrian loading conditions was implemented by finite element simulations regarding three influencing factors: impact heights, locations of impact and impact velocities.

Résultats marquants :** **Knee joint injury criteria (combining shearing and bending) and validated with pedestrian tests

The injury thresholds associated with primary knee ligament injuries of pedestrians were defined with the dominant injury mechanisms: combined lateral bending and shearing effects. These thresholds are also well correlated with the previous criteria defined by isolated lower limb tests.

Chapitre 2 : *Incidence du design de la face avant du véhicule sur la vulnérabilité du membre pelvien*

Ce chapitre est présenté sous la forme d'un article intitulé « Evaluation of injury thresholds of lower extremities by FE simulations of full-scale vehicle-pedestrian impacts » par Fuhao Mo, Massimiliano Avalle, Alessandro Scattina, Elena Semino, Catherine Masson, Pierre Jean Arnoux en cours de révision à l'international Journal of Crashworthiness.

OBJECTIVE: The present study work aims to investigates by simulation incidences the influence of four various different passenger vehicle front end structures on general injuries of a biofidelic pedestrian lower extremities by finite element simulations, under the impact speed of 40 km/h that is used in the passenger vehicle-pedestrian crash test of the European currently used for pedestrian safety regulation.

METHOD: Using a detailed finite element model of the lower limb, this work was focused on the evaluation of tibia fractures and knee ligament ruptures were concerned in the present study. The Influences of vehicle front end structures on the risk of these two injury occurrences were investigated by finite element simulations using a biofidelic lower limb model and various passenger vehicle models. using 4 Four passenger vehicle types were involved: Super Mini (SM), Small Family Car (SFC), Executive Car (EC), and Multi Purpose Vehicle (MPV) passenger vehicle types. Knee ligament strains and tibia bending moments were measured computed in order to postulate on to indicate injury risk occurrences of the corresponding structures. Additional lower extremity kinematics during the impact was also recorded to find study incidences of various vehicle front end designs on these injuries.

RESULTS: Reported results showed the influence of Various vehicle front end designs show their influences on lower extremity kinematics and, injury risk of the knee ligaments and tibia bone structure. By comparing the injury risk of both knee ligaments and tibias, theAccording to the different vehicle models tested, the differences in bumper beam design is indicated as an important factor that influences above injuries, such asas also including the bumper beam height, width in the height direction, the deformable depth between it and the bumper fascia should be considered in the vehicle design to mitigate lower extremity injuries.

***Résultats Marquants** : The incidences influence of various vehicle front end structures on knee ligaments and tibia injuries indicated by overall results can provide valuable information to improve the current vehicle front end design for pedestrian protection.*

Chapitre 3 : Evolutions des critères de blessure de la tête

Ce chapitre est dédié à l'évolution des critères de blessure de la tête qui distingue les lésions osseuses des lésions de la matière cérébrale. L'énergie de déformation de la structure osseuse semble un bon indicateur de la fracture du crâne, les hématomes sous duraux semblent être bien corrélés avec l'énergie de déformation de l'espace sub-arachnoïdien et les lésions neurologiques sont décrites à partir du calcul des contraintes et des déformations de cisaillement du cerveau.
L'analyse proposée ici vise à renforcer la robustesse des modèles existants. Elle combine analyse par éléments finis et analyse par simulations multi corps, analyse de sensibilité et reconstruction d'accidents réels.

Résultats marquants :

La reconstruction d'accidents réels a permis de montrer que l'évaluation des contraintes de Von Mises est un bon prédicteur du risque de lésion axonale diffuse.
La modélisation des profils de rupture du pare-brise contribue à une modélisation bio-fidèle des fractures de la boite crânienne. L'influence de l'âge, de la morphologie de la boite crânienne ont été intégrées dans le modèle SUFHEM et le calcul des critères de blessure (chez l'adulte).
La variabilité des propriétés mécaniques de la matière cérébrale a pour effets une variation très significative des contraintes de cisaillement et de la localisation de ces maxima. Il en découle que les limites de tolérance en termes de contraintes de cisaillement intracérébrales basées sur la modélisation par éléments finis dépendent de la modélisation de la loi de comportement du cerveau (laquelle exhibe des différences très significatives dans la littérature).
L'accélération angulaire lorsqu'elle est prise en compte montre une grande incidence sur le cisaillement intracérébral. Ces résultats supportent la mise en place de capteurs rotatoires dans les têtes de mannequins lors d'essais expérimentaux.

Sommaire

Chapitre 1
Evolutions des critères de blessure de la jambe ***244***

I. Injury tolerance of tibia for the car–pedestrian impact *244*

II. Coupling Lateral Bending and Shearing Mechanisms to Define Knee Injury Criteria for Pedestrian Safety *256*

III. Investigation of the injury threshold of knee ligaments by the parametric study of car-pedestrian impact conditions *272*

Chapitre 2
Incidence du design de la face avant du véhicule sur la vulnérabilité du membre pelvien ***291***

I. Matériels et méthodes *292*

II Résultats *293*

III Discussion & Conclusion *297*

IV Conclusion *298*

Références *298*

Chapitre 3
Critères de blessure du segment céphalique ***301***

I. Introduction *301*

II. Reconstruction d'accidents réels et évaluation des critères de blessure de MEF SUFEHM *302*

III. Conclusion *311*

Chapitre 1 :

Evolutions des critères de blessure de la jambe

I. Injury tolerance of tibia for the car–pedestrian impact

This article is published in the journal- Accident Analysis and Prevention:
Mo F, Arnoux PJ, Jure JJ, Masson C. Injury tolerance of tibia for the car–pedestrian impact. Accident Analysis & Prevention. 2012; 46(0):18-25.

INTRODUCTION

The pedestrian is one of the most vulnerable road users around world, in overall France, the 2008 accidental data show that pedestrian injuries accounted for approximately 13.6% of total traffic road injuries, with 580 fatalities of these victims (ONISR 2009). Although rarely fatal, lower limbs have been found in many studies to be the most common injured body part of pedestrians, followed by the head injuries as a close second (IHRA 2001,Cater et al., 2008). Moreover, it was also reported that lower limbs injuries of pedestrians cost cumulatively more than any other body regions (Richards et al., 2009). In addition, lateral blunt impact with the bumper has been identified as the most common cause for tibia injuries (Yang 2005). However, the detailed influence of bumpers on the tibia structural response is still unknown.

The bending tolerance of tibia bone structure has been globally reported in the previous studies. For example, Yamada (1970) summarized tibia static bending tests conducted by Motoshima in 1960 with average fracture tolerance 184 Nm, which indicated that the female has five-sixths tibia bending strength of the male, and the fracture bending moment varies negligibly between the anterior-posterior and lateral-medial direction. In the reported tests of this study, the significant variances of bending tolerance due to impact directions were also not found. For dynamic bending, Nyquist et al. (1985) reported that mid-shaft fracture of the tibia occurred at bending moments of about 280 and 320 Nm for females and males, respectively, regardless of the impact directions. And Nyquist et al. (1985) also indicated that X-ray films of pedestrian victims commonly show classical tibia fracture patterns similar to bending failures of brittle beams. Hence, tibia bone structure could be assumed as a simple cylindrical beam under bending regardless of loading directions. In addition, according to recent studies (Ivarsson et al., 2004, 2005), the loading responses of the legs to lateral-medial bending depended highly on loading locations. Thus, research on tibia tolerances of different locations could be necessary.

Several tibia injury risk functions were developed from the previous test results. Mertz (1993) summarized the tibia injury criteria, and indicated that tibia index was an injury risk function considering combined bending and axial compressive loading on tibia. Then, the revised tibia index was developed from the tibia index equation based on bending test data in the literature (Nyquist et al., 1985,Schneider, Crandall 1997). Recently, Kerrigan et al. (2004) scaled the dynamic three-point bending test data from several studies based on reference geometry to develop injury risk functions for pedestrian lower extremities. However, only test data from dynamic mid-shaft bending were included in the injury risk function of leg, and the influence of scaling method was also not been discussed. The validity of these injury risks functions could not remain available when bending appears elsewhere on tibia. In addition, regarding

pedestrian real impact conditions, tibia tolerance of different locations should be also balanced according to vehicle front end structure (Kuwahara et al., 2007,Thollon et al., 2007).

The current study aims to investigate the fracture response and define injury tolerance of tibia bone structure loaded at three-point bending and car-pedestrian impact conditions.

- From experimental data, eleven quasi-static bending tests of tibia mid-shaft performed in our laboratory and additional literature data of Kerrigan et al. (2003a, 2003c, 2004) were used to define the injury risk functions of tibia bone structure. The study of Kerrigan et al. (2004) included the experimental data from Kerrigan et al. (2003a, 2003c, 2004). Under the assumption of beam theory, the injury risk functions for quasi-static and dynamic bending were defined through Weibull survival model respectively.
- To investigate the relevancy of injury risk functions, furthermore, the influence of bone locations on bending tolerance, both three-point bending and car-pedestrian impact conditions were simulated using finite element model of lower limbs. Numerical simulations showed that locations could lead to significant variances of tibia fracture moment with maximum tolerance around mid-shaft.

MATERIELS & METHODS

Experimental tests

Eleven tibias were obtained from cadavers with ethical guidelines and research protocol approved by Laboratoire de Biomécanique Appliquée (Jundt 2007). The specimens were loaded at quasi-static three-point bending from three different directions (Anterior-posterior, Posterior-Anterior and Lateral-Medial) (Appendix Table A.4). Prior to testing, all specimens were measured based on the anthropometric and anatomic structure. The experimental test consisted to put bone extremities into cement moulds. Then, Specimens were mounted in the experimental apparatus by set the bone moulds on cylindrical supporters in the correct loading directions. A cylindrical impactor with 20 mm diameter attached to the crosshead of the experimental machine was lowered for pre-contact with bone at about 10-20N. Then the test machine was imposed with the imposed velocity at 76mm/min. The electronic data including impactor force and displacement were sampled at 10, 000 Hz.

Injury risk function

Under the assumption of three-point bending theory, the bending moment can be estimated by the equation as follows:

$$M_{peak} = PL/4 \qquad \text{(Erreur ! Il n'y a pas de texte répondant à ce style dans ce document..1)}$$

Where P is the peak force of impact, and L is the span between the two supporters. As assuming that tibia can be modeled as a linear beam, based on beam theory, the peak stress is proportional to the peak moment as equation 4.2:

$$\sigma_{peak} = M_{peak} C / I \qquad \text{(Erreur ! Il n'y a pas de texte répondant à ce style dans ce document..2)}$$

where I is the moment of inertia of the cross section and C is the peak value of distance from neural axis associated with stress. Hence, under the assumption that the tibia shaft has the same failure peak stress, the fracture moment can be scaled through the reference geometry to develop the injury criteria regarding some geometric characteristics. The scaling method used in this study has been developed in Kerrigan et al. (2004).
Typically, the tibia length of 50th percentile is adopted as reference length. Diffrient's study indicated the length of medium tibia is 411mm (Diffrient et al., 1993). And the tibia length of

LLMS (Lower Limb Model for Safety) model (406.5mm) from 50% human volunteer approximated to Diffrient's statistic result. Thus, in this study, the tibia length of LLMS model would be taken as the reference length for better comparison of experimental tests and simulations. Furthermore, the reference tibia supporting span for two moulds was defined as 313 mm for the tibia model of LLMS through the experimental reality. Therefore, tibia moments in the tests were scaled to the reference geometry through a scale factor (λ_L), and equations, as follows:

$$\lambda_L = L_{ref} / L$$ (Erreur ! Il n'y a pas de texte répondant à ce style dans ce document..3)

$$M_{peak-scaled} = \lambda_L^3 M_{peak}$$ (Erreur ! Il n'y a pas de texte répondant à ce style dans ce document..4)

where $M_{peak-scaled}$ is scaled fracture moment, M_{peak} is the fracture moment evaluated from the test data, L_{ref} and L are the reference length and real length (including the tibia length, and the span between two supporters) measured from the test, respectively. Experimental data reported in this study were scaled by the reference span regarding the experimental information. The previous data from Kerrigan et al. (2003a, 2003c, 2004) were scaled by the reference tibia length.

Then, the parametric injury risk functions of tibia were developed from the test data using Weibull survival model. The probability of bone fracture as a function of fracture moment is given by:

$$\Pr ob(fracture) = 1 - \exp(-\exp(A\ln(M) - B)$$ (Erreur ! Il n'y a pas de texte répondant à ce style dans ce document..5)

where A and B are the specific parameters of Weibull survival model, and M is M_{peak} (fracture moment) or $M_{peak-scaled}$ (scaled fracture moment through M_{peak}).

Finite Element Simulation

"Lower Limb Model for Safety" (LLMS) model was selected for the simulation analysis (Figure 4.1), which is a finite element model developed from 50th percentile human male. The whole details of LLMS model has been reported largely by published studies from design to validation (Arnoux 2000,Beillas et al., 2001,Arnoux et al., 2005). In this study, the LLMS model was applied on two loading conditions as follows:

-Under the same boundary condition with the bending test reported in this study, the tibia model extracted from LLMS model was loaded at lateral-medial direction under quasi-static and dynamic loading (Figure 4.1.a). The same dynamic bending velocity at 1.5m/s in the Kerrigan et al. (2004) test was selected in this study, because the bone strain rate loading at 1.5m/s three-point bending is commensurate to the rate experienced by pedestrian struck by a vehicle moving at 40km/h through the simulation.

-Under the car-pedestrian impact condition, a "Euroncap supermini (segment B)" class finite element car model and the pedestrian model were included (Figure 4.1.b). The vehicle model had an initial velocity at 11.1m/s. The pedestrian model was the combination of the 50% Hybrid-III dummy model and LLMS model at hip joint in the lateral impact direction with vehicle to consider the whole human body inertial effects during impact sequence. As shown in the Appendix (Figure A.3), the lower limb kinematics in the simulation had good correlations with the experimental test results (Masson et al., 2007).

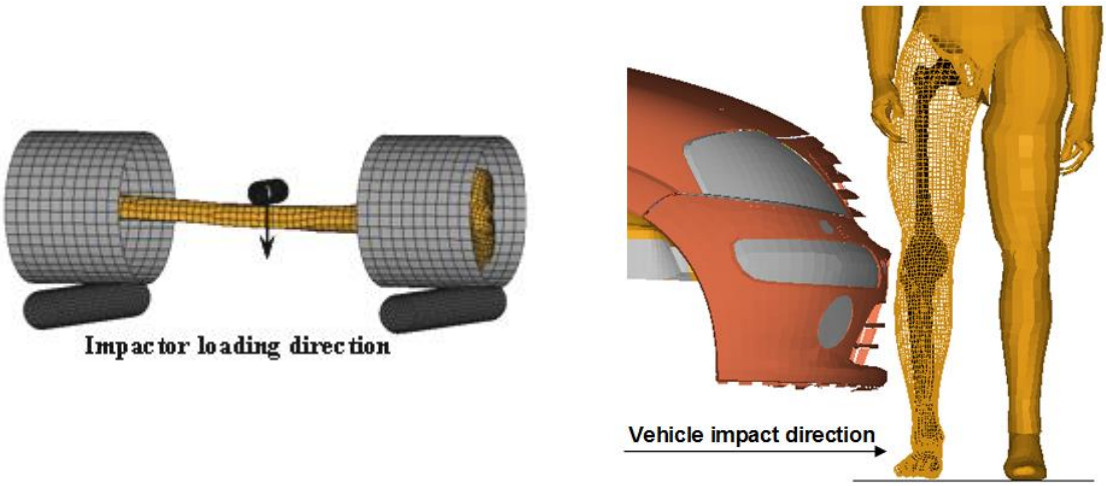

(a) Lateral-Medial bending model of tibia **(b) car-pedestrian impact model**

Figure Erreur ! Il n'y a pas de texte répondant à ce style dans ce document.**.1 Descriptions of FE models**

From prox 1/3 to dist 1/3 (1/3 tibia length from the proximal end and distal end of the tibia), eleven loading locations of impactor with averaged interval 13.6 mm were selected to evaluate the influence of impact locations (P0-P10 as symbols for 11 sections, P0 – prox 1/3, P5 – mid-shaft, P10 – dist 1/3). Regarding the car-pedestrian impact, bumper is the main component implementing the loading on lower limbs of pedestrian. To load tibia bone structure at the same locations with three-point bending simulations, the pedestrians were translated to make these tibia locations at the same height with bumper beam center. Figure 4.2 shows the locations of prox 1/3, mid-shaft and dist 1/3 as examples.

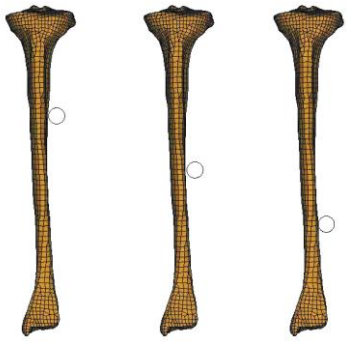

Figure Erreur ! Il n'y a pas de texte répondant à ce style dans ce document.**.2 Impact locations from left to right: prox 1/3, mid-shaft and dist 1/3**

Bending moment diagrams were depicted through sections defined around each layer of tibia elements with mean interval about 6.5 mm along the tibia axial direction according to the element size. Totally, there are 62 sections for tibia in the car-pedestrian crash model and 32 sections in the three-point bending model (because of the rigid body mount conditions, only the section from prox 1/3 to dist 1/3 were considered) for calculating the bending moment at each cross-section.

RESULTS

Injury tolerance definition from experimental data

Both quasi-static and dynamic injury risk functions were defined using fracture moments from the test data of our lab and previous literatures (Kerrigan et al., 2003a,Kerrigan et al., 2003c,Kerrigan et al., 2004,Jundt 2007), respectively. The detailed data obtained were reported in the Appendix (Table A.4 and A.5).

Therefore, according to both dynamic and quasi-static loading conditions investigated, four injury risk curves considering quasi-static/dynamic bending and non-scaled/scaled moments were shown in Figure 4.3. Then, Table 4.1 lists the summary results of the injury risk functions. The null hypothesis is that the data follow the Weibull distribution. Kolmogorov-Smirnov test was used to check relevancy if the test data following the Weibull distribution. The p-value, in contrast to Kolmogorov-Smirnov critical values, indicates the threshold value of the significance level in the sense that Weibull distribution assumption can be accepted for all significance levels less than the p-value. From the results, Kolmogorov-Smirnov values are smaller than critical value (0.391) at 5% significant level and p-value higher than 0.05 (Table 4.1), which indicate that the Weibull distribution of data can be accepted.

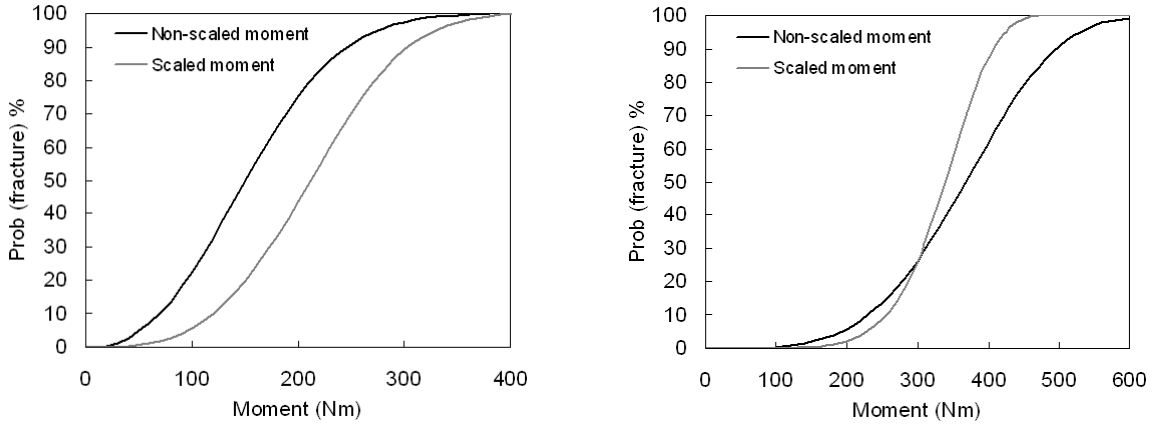

(a) quasi-static bending **(b) dynamic bending**

Figure Erreur ! Il n'y a pas de texte répondant à ce style dans ce document..**3 Injury risk curves of (a) quasi-static and (b) dynamic bending based on the Weibull survival model. Prob(fracture) indicates the probability of tibia fracture corresponding to the moment.**

Then, 50% fracture possibility of risk functions could be defined as the injury tolerances for tibia bone structure. The difference of tibia tolerances between quasi-static and dynamic bending is significant from Figure 4.3 and Table 4.1. The scaling method increased the failure moment of 50% fracture possibility for quasi-static bending data from 150 Nm to 212 Nm, however, it decreased slightly this value from 369 Nm to 339 Nm for dynamic loading.

Table Erreur ! Il n'y a pas de texte répondant à ce style dans ce document..**1 Descriptions of injury risk functions (Prob 50% fracture moment indicates the moment corresponding to 50% probabilities of tibia fracture based on the injury risk functions)**

Test types	Data processing	A	B	Prob 50% fracture moment (Nm)	Kolmogorov-smirnov test	P-value
Quasi-static bending	Non scaled	2.4449	12.6233	150	0.1944	0.7324
	Scaled	3.3239	18.1893	212	0.1664	0.8730
Dynamic	Non scaled	4.0265	24.1531	368	0.2251	0.5591

bending	Scaled	6.6553	39.1462	339	0.1916	0.7476

Injury tolerance definition from numerical simulations

Three-points bending

Typical curves of section moment to section distance from tibia plateau when the fractures occurred were shown in Figure 4.4 (prox 1/3, mid-shaft and dist 1/3). For the impact at eleven locations, the peak moments and fracture could be found around impactor loading regions. The fractures could also occur around prox 1/3 at the same time. The large variations of fracture moment diagrams from these three locations can be found in the Figure 4.4. For example, in the dynamic loadings, the peak moments are 187 Nm, 326 Nm and 277 Nm for prox 1/3, mid-shaft and dist 1/3, respectively (Figure 4.4.b).

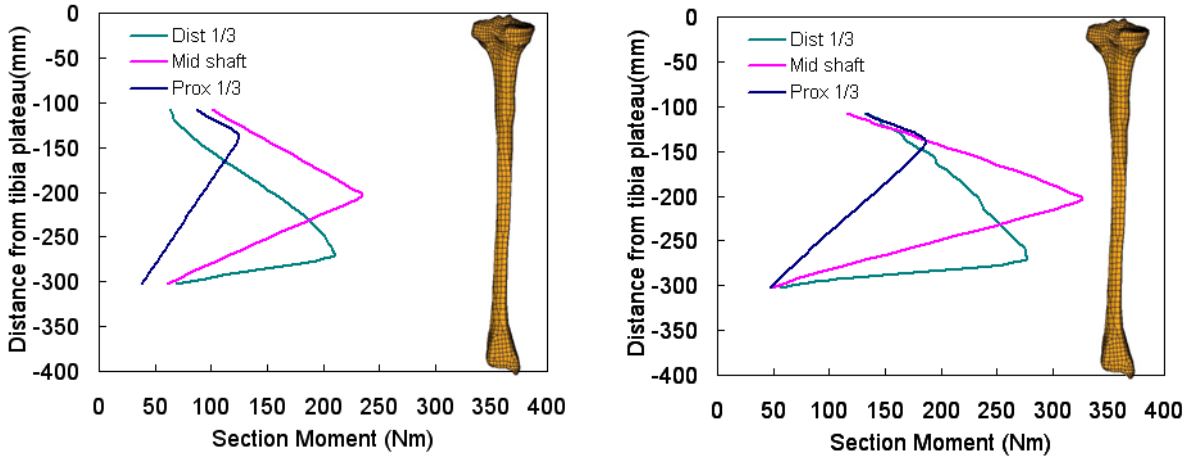

(a) quasi-static bending **(b) dynamic bending**

Figure Erreur ! Il n'y a pas de texte répondant à ce style dans ce document.**.4 Diagrams of section moments when the fractures occur in the (a) quasi-static bending and (b) dynamic bending simulations.**

Furthermore, as shown in Figure 4.5, although with the same failure stress, the peak section moments when fracture occurred were recorded for the impacts at different locations, which varied largely from prox 1/3 to dist 1/3. The variances of tibia peak moments between dynamic and quasi-static loading are also significant in different locations. As shown in the results, the maximum fracture moment between prox 1/3 and dist 1/3 is closed to mid-shaft at P6 with 248 Nm and 380 Nm for quasi-static and dynamic loadings respectively, in contrast to the minimum located at prox 1/3 (125 Nm for quasi-static loading and 187 Nm for dynamic loading). As the distance from P6 increases, the fracture moment decreases gradually. To globally understand the tibia strength between prox 1/3 and dist 1/3, the regressive curves for these peak moments were also reported (Figure 4.5). The regressive functions were listed in the Table 4.2 with good R square values.

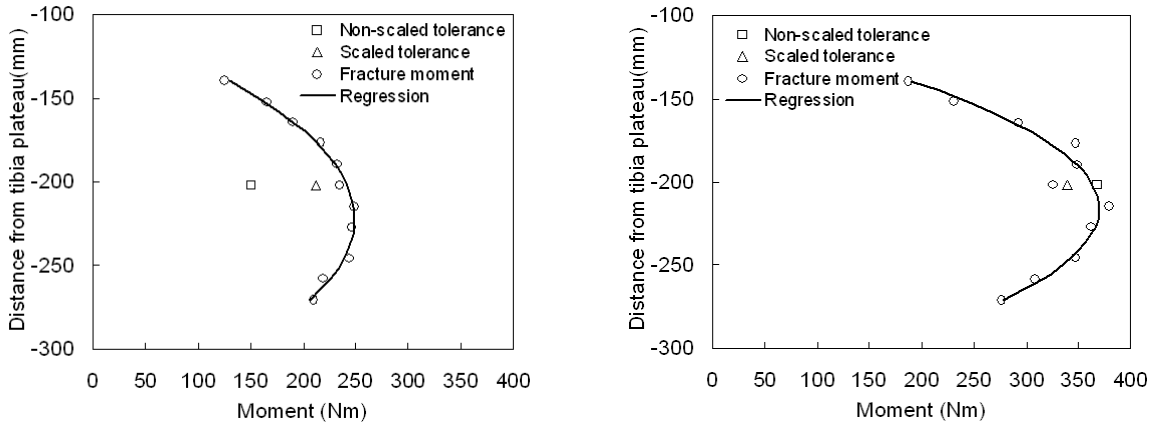

(a) quasi-static bending **(b) dynamic bending**

Figure Erreur ! Il n'y a pas de texte répondant à ce style dans ce document..**5 Fracture moments of different locations in the (a) quasi-static bending and (b) dynamic bending simulations.**

To compare with the injury risk functions defined from the experimental tests, the moment corresponding to 50% probability of tibia fracture were considered as the injury tolerances (Table 4.1). As shown in Figure 4.5, regardless of quasi-static and dynamic bending, scaled tolerance is more closed to the mid-shaft fracture moment (P5: 235 Nm and 326 Nm for quasi-static and dynamic loadings respectively) in the simulations.

Table Erreur ! Il n'y a pas de texte répondant à ce style dans ce document..**2 Descriptions of regressive curves (d represents the distance from tibia plateau to impactor center and Mpeak is the peak moments when the fractures occur)**

Test types	Regression functions	R2
Quasi-static bending	$M_{peak} = -0.0175d^2 - 7.77d - 613.98$	0.99
Dynamic bending	$M_{peak} = -0.0307d^2 - 13.27d - 1064.8$	0.93

Car-pedestrian crash

Considering full pedestrian kinematics (Figure 4.6), the maximum value of section moments through whole tibia occurred around the tibia area with bumper beam loading regardless of the appearance of fracture or not. The fibula fracture located at the region corresponding to the direct bumper loading, however, the fracture of tibia was always found around prox 1/3 region for the impacts from P0 to P5.

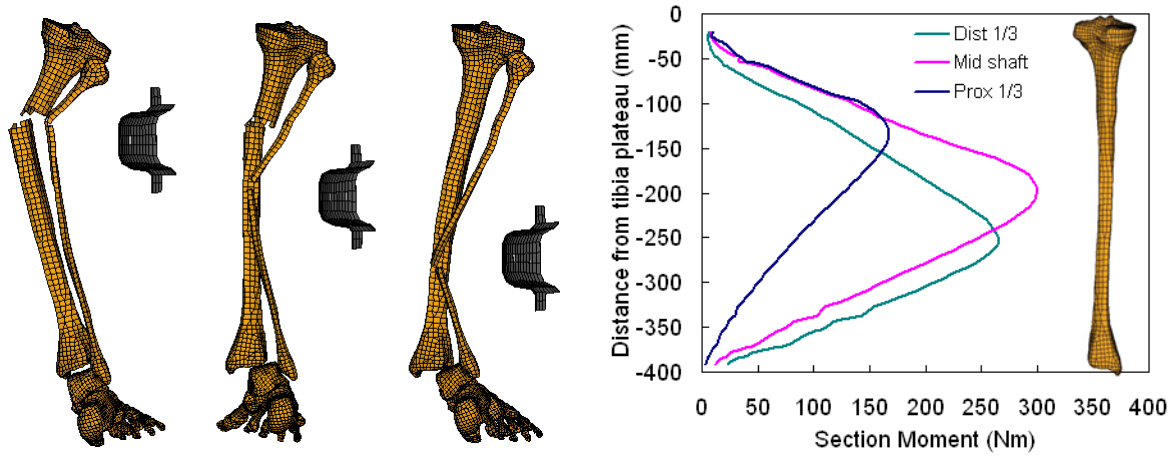

(a) dynamics of prox 1/3, mid-shaft and dist 1/3 impacts

(b) diagram of tibia section moments

Figure Erreur ! Il n'y a pas de texte répondant à ce style dans ce document.**.6 Typical car-pedestrian simulations: (a) dynamics of prox 1/3, mid-shaft and dist 1/3 impacts and (b) diagram of tibia section moments.**

Thus, to consider the variation of tibia fracture moments found in the three-point bending simulations, the regressive curve (Figure 4.5.b) from dynamic three-point bending simulations was used to evaluate the possible fracture of tibia for car-pedestrian impacts. In the simulations, six impacts from location P0 to P5 suffered from fractures around prox 1/3 region. As shown in the Figure 4.7.a, the section moments at prox 1/3 location of these impacts with fracture all exceeded the tolerance (189 Nm) of regressive curve apart from P0, and the moments of other regions without fracture were lower than the tolerance. The section moment of P0 impact at prox 1/3 is 167 Nm approximated to the tolerance.

From the diagram of impacts without fracture (Figure 4.7.b), most of section moment curves were below the injury tolerance curve apart from P6. The prox 1/3 section moment (213 Nm) of P6 impact slightly exceeded the limitation (189 Nm) but without fracture.

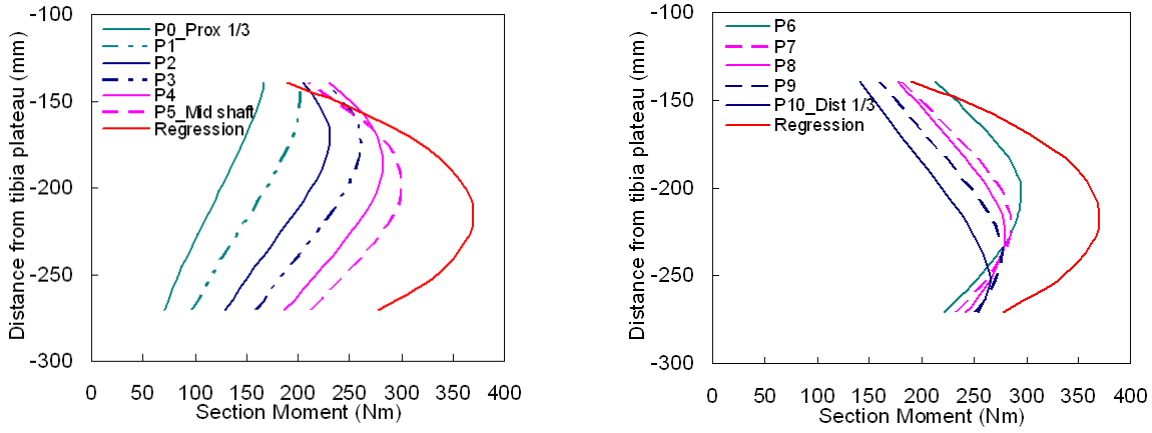

(a) with tibia fractures

(b) without tibia fractures.

Figure Erreur ! Il n'y a pas de texte répondant à ce style dans ce document.**.7 Evaluations of the car-pedestrian simulations (a) with tibia fractures and (b) without tibia fractures.**

DISCUSSION

The current study investigated the tibia tolerance of bending moment at fracture regarding tibia length, section properties and locations, with combined experimental tests and finite element simulations. Previous studies have assessed tibia tolerance and develop injury risk functions mainly through mid-shaft bending tests (Nyquist et al., 1985,Kerrigan et al., 2004). Through the dynamic leg bending tests, Ivarsson et al. (2005) indicated the structural response to lateral-medial 3-point bending is highly dependent on loading location. From simulations in this study, the significant variation of tibia fracture moment under lateral-medial bending has been found from prox 1/3 to dist 1/3. And the P6 location closed to mid-shaft had the maximum tolerance in this region of tibia. Based on the modeling characteristics, the cross-section property especially the thickness of compact bone varies with the locations, which could be responsible for this variation. It indicates that the tibia tolerance should be developed for different impact locations and their corresponding diversity of the cross-section property.

In addition, the three point bending boundary condition could have influence on these variances, and it should be considered in setting up the injury tolerance for pedestrian. Because the similar section moment curve contours between isolated three-point tibia bending (Figure 4.4.b) and car-pedestrian crash (Figure 4.6.b) could indicate the similar tibia boundary conditions for both loading situations. In the car-pedestrian simulation, the leg was loaded by car bumper, and showed its lateral bending around knee joint and ankle joint, which is closed to three-point bending around two supporting cans. And the lower limbs impact happens in very short time, the gravity influence could be negligible. Hence, the injury tolerance developed from pure tibia bending could be considered as the proper criteria, which can be applied to evaluate the tibia injury risk for the car-pedestrian crash.

Hence, to consider the influences of impact locations according to tibia section property, the regression of bending moments at fracture can be implemented through simulations. In the current study, fracture bending moments at eleven locations were used to develop the regressive curve. Then, the tolerance of tibia risk function can be scaled based on this type of regressive function to predict the bone fracture regarding location, section property and tibia length. In this study, since the mid-shaft fracture moment of regression curve is similar to the tolerance (the moment corresponding to 50% possibility of fracture) of dynamic injury risk function, the regressive function has been directly used for predicting the tibia fracture in the car-pedestrian simulation. Such investigations could be improved with an enlarged tibia tolerance evaluation at different impact locations. From the evaluations of car-pedestrian simulations, most of simulations followed the regression tolerance developed from three-point bending simulations well apart from P0 and P6 locations. The possible reason could be due to similar but not the same loading conditions. In addition, the high frequency and low tolerance of the prox 1/3 location from simulations could be due to the model definition with a very thin compact bone around this location, and very closed to metaphysis structure modeling with combination of spongy and compact bone (solid and shell elements) for considering the anatomic structure. Because the significant differences can be found in the biomechanical properties between the diaphysis and metaphysis, the metaphyseal structure has a relatively thin cortex with a fairly significant intramedullary supporting structure of cancellous bone. Therefore, improving tibia model with detailed geometric structure could be available for more accurate prediction of fracture.

Furthermore, from the whole bending moment calculation through tibia sections, the maximum value of bending moment were located at the same heights that impact with the

vehicle bumpers. Thus, it indicates the tibia region with direct loading from vehicle could be most vulnerable region with possible tibia fracture from prox 1/3 to dist 1/3. IHRA (2001) showed that the bumper center height of sedan is typically about 476 mm, which is closed to 500 mm of the 50th tibia plateau height (Diffrient et al., 1993). So it could indicate the crash between 50% pedestrian and this type of sedan more likely lead to tibial metaphysis or proximal tibia fractures. And from the analysis of fracture moments due to locations, the prox 1/3 could be the most fragile region between prox 1/3 and dist 1/3 of tibia. Thus, according to the existing vehicle structure, the prox 1/3 of tibia could be more easily impacted with bumper and suffered from serious injuries in the region from prox 1/3 to dist 1/3.

Again, in this study, quasi-static bending of eleven tibias in the mid-shaft has been reported to make comparisons with previous studies. The tibia specimens were conserved with Winckler (1974) solution to ensure proper preservation of bone tissues. Regarding embalmed cadaver bone mechanical behaviour, Crandall (1994) showed that the conservation with a similar Winckler solution did not have a significant incidence on the tissue mechanical response. Average 164 Nm of bending moment at fracture was in agreement with the literatures (Yamada 1970,Nyquist 1986). To evaluate tibia tolerance under car-pedestrian impact condition and compare with quasi-static test data in the current study, dynamic leg bending data collected from the recent literatures were also used to develop injury risk functions. The flesh and fibula structure of leg can be supposed without significant influence on tibia fracture moment because of the limited stiff, which was also found in our simulations. To strengthen these current assumptions, coupled simulation and experimental tests could be performed in a further step, to investigate surrounding tissues and structure contribution to tibia failure risk. Weibull survival model was selected to develop injury risk functions of tibia through the reported test data and additional data from literatures. Because it has been largely applied on analyzing the small number data sample and also been indicated properly for developing biomechanical injury risk curve (Kent 2004). In addition, the test data following Weibull distribution were well accepted in statistics through goodness of fit test. In the comparison of both quasi-static tibia and dynamic leg injury functions, the large difference between two types of injury risk functions seems to indicate the significant strain rate. And in the three-point bending simulation, the failure moment of bone under dynamic bending increases largely compared with the quasi-static bending, which also indicates the significant sensitivity of injury tolerance to strain rate.

From the results, the differences in the injury risk functions between non-scaled moments and scaled moments can be found. It indicates that the scaling method relevant with bone property lead to significant variation on the prediction of fracture. The scaled test data seems to be more convergent and better following Weibull distribution. This point could be relevant with some extreme data which have been scaled to be close to standard value based on the reference geometry (Appendix Table A.4 and A.5). The introduction of scaling method considering section properties could bring in a better evaluation of fracture risk according to the simulation results. However, the scaling method relates to the tibia reference length as well as the uniform failure stress assumption that could be one drawback. The bone fracture stress could vary to some extent because of the microstructure and mineral content of different tibia. And the proper reference geometries should be selected according to the statistical data of literatures.

With the development of modern automobile industry, the pedestrian safety is more and more concerned by all stakeholders including road users, researchers, legislators and manufacturers. The injury tolerance developed in the current study can be used as the criteria to sustain the

development of safer car front-end structure and promote new standards for design and regulations. However, based on the traffic epidemiology of real accidents (IHRA, 2001), only lateral impact with most frequencies (80-90 percent) was considered in the current study. Additionally, many factors could influence the car-pedestrian impact and induce tibia injuries. Some factors are related to the pedestrian with material properties, for example, age, osteoporosis, tibia size, etc; other factors concern boundary conditions including the impact speed, impact location on the tibia, impact direction, etc. The current paper principally investigated the influences of impact locations on the tibia tolerance with typical 50% pedestrian model. Thus, the influences of age and corresponding bone properties were not explored at this stage. In the future, the robustness of the current tibia tolerance should be improved by both experimental test and numerical simulation regarding variability of those other important factors.

CONCLUSION

Eleven tibia tests under quasi-static three-point bending were reported in the comparison with other dynamic bending data from literatures. Based on the Weibull survival model, the injury risk curves of tibia under quasi-static and dynamic three-point bending were developed. Both the scaling method and strain rate have significant influence on developing the injury risk functions. The scaling method could be available way to consider the bone size influence on the tibia fracture moment. The typical values of mid-shaft fracture (50% fracture probability) are 212 Nm for quasi-static bending and 339 Nm for dynamic bending from scaled injury risk functions, respectively.

The fracture moment of tibia varies largely from prox 1/3 to dist 1/3 under bending condition. Thus, the bending injury tolerance developed from the mid-shaft could not be applied on the other regions directly for pedestrian. To consider the tibia tolerance at different locations, an injury tolerance curve obtained from regression (numerical simulations) was shown to be available to evaluate the tibia fracture for car-pedestrian impacts. Furthermore, the tibia tolerances of different locations are necessary to be explored for car-pedestrian impacts in the future through experimental tests.

REFERENCES

Arnoux, P.J., 2000. Modélisation des ligaments des membres porteurs. Ph.D. thesis. Université de la Méditerranée.

Arnoux, P.J., Cesari, D., Behr, M., Thollon, L., Brunet, C., 2005. Pedestrian lower limb injury criteria evaluation: A finite element approach. Traffic Injury Prevention 6 (3), 288–297.

Beillas, P., Arnoux, P.J., Brunet, C., Begeman, P., Cavallero, C., Yang, K.H., King, A., Kang, H.S., Kayvantash, K., Prasad, P., 2001. Lower limb: advanced fe model and new experimental data. Stapp Car Crash Journal 45 (November), 469–494.

Cater, E.L., Neal-Sturgess, C.E., Hardy, R.N., 2008. APROSYS in-depth database of serious pedestrian and cyclist impacts with vehicles. International Journal of Crashworthiness 13 (6), 629–642.

Crandall, J., 1994. Preservation of human surrogates for impact studies. Ph.D. thesis. University of Virginia.

Diffrient, N., Tiley, A., Harman, D., 1993. Humanscale. The MIT Press, Massachusetts Institute of Technology, Cambridge, MA.

International Harmonized Research Activities (IHRA), 2001. Pedestrian safety working group 2001 report.

Ivarsson, B., Kerrigan, J., Lessley, D., Drinkwater, D., Kam, C., Murphy, D., Crandall, J., Kent, R., 2005. Dynamic response corridors of the human thigh and leg in non-midpoint three-point bending. 2005 SAE World Congress, Detroit, MI, USA.
Paper No. 2005-01-0305.
Ivarsson, B., Lessley, D., Kerrigan, J., Bhalla, K., Crandall, J., Kent, R., 2004. Dynamic response corridors and injury thresholds of the pedestrian lower extremities. In: Proceedings of the 2004 International IRCOBI Conference, Graz, Austria, pp. 171–191.
Jundt, G., 2007. Modéles d'endommagement et de rupture des matériaux biologiques. Ph.D. thesis. Université de la Méditerranée.
Kent, R., Funk, J., 2004. Data censoring and parametric distribution assignment in the development of injury risk functions from biomechanical data. 2004 SAE World Congress, Detroit, MI, USA. Paper No. 2004-01-0317.
Kerrigan, J., Bhalla, K., Madeley, N., Funk, J., Bose, D., Crandall, J., 2003. Experiments for establishing pedestrian-impact lower limb injury criteria. 2003 SAE World Congress, Detroit, MI, USA. Paper No. 2003-01-0895.
Kerrigan, J., Bhalla, K., Madeley, N., Funk, J., Crandall, J., Deng, B., 2003b. Response corridors for the human leg in three-point lateral bending. In: Proceedings of the 7th US National Congress on Computational Mechanics, Albuquerque, NM, USA, Paper No. 1281.
Kerrigan, J., Drinkwater, D., Kam, C., Murphy, D., Ivarsson, B., Crandall, J., Patrie, J., 2004. Tolerance of the human leg and thigh in dynamic latero-medial bending. International Journal of Crashworthiness 9 (6), 607–623.
Kuppa, S., Wang, J., Haffner, M., Eppinger, R., 2001. Lower extremity injuries and associated injury criteria. In: Proceedings of the 17th International Technical Conference on the Enhanced Safety of Vehicles Conference (ESV), Amsterdam, The Netherlands, Paper No. 457.
Kuwahara, S., Hosokawa, T., Keita, O., Mizuno, K., 2007. Finite element analysis of pedestrian lower extremity injuries in car-to-pedestrian impacts. In: 2007 SAE World Congress, Detroit, MI, USA, Paper No. 2007-01-0755.
Masson, C., Serre, T., Cesari, D., 2007. Pedestrian-vehicle accident: Analysis of 4 full scale tests with pmhs. In: Proceedings of the 20th International Technical Conference on the Enhanced Safety of Vehicles Conference (ESV), Lyon, France, Paper No. 07-0428.
Nyquist, G.W., 1986. Injury tolerance characteristics of the adult human lower extremities under static and dynamic loading. In: SAE World Congress, Paper No. 861925.
Nyquist, G.W., Cheng, R., Ei-Bohy, A., King, A., 1985. Tibia bending: strength and response. In: SAE World Congress, Paper No. 851728.
Obervatoire National Interministériel de la Sécurité Routière (ONISR), 2008. Road safety in France: absract of the 2008 report.
Richards, D., Cookson, R., Cuerden, R., Davies, G., 2009. Prioritising pedestrian injury prevention based on frequency and cost. In: Proceedings of the 2009 International IRCOBI Conference, York, UK, pp. 223–236.
Schneider, L., Crandall, J., 1997. Static and dynamic bending strength of the leg. In: Proceedings of the 1997 International IRCOBI Conference, Hannover, Germany, pp. 99–113.
Thollon, L., Jammes, C., Behr, M., Arnoux, P.J., Cavallero, C., Brunet, C., 2007. How to decrease pedestrian injuries: conceptual evolutions starting from 137 crash tests. Journal of Trauma-Injury Infection and Critical Care 62 (2), 512–519.
Winckler, G., 1974. Manuel d'Anatomie Topographique et Fonctionnelle, 2ème ed. Masson, Paris.
Yamada, H., 1970. Strength of Biological Materials. Williams and Wilkins, Baltimore.
Yang, J.K., 2005. Review of injury biomechanics in car–pedestrian collisions. International Journal of Vehicle Safety 1 (1/2/3), 100–117.

II. Coupling Lateral Bending and Shearing Mechanisms to Define Knee Injury Criteria for Pedestrian Safety

This article is published in Traffic Injury Prevention Journal : Fuhao M, Masson C., Arnoux PJ., Coupling Lateral Bending and Shearing Mechanisms to Define Knee Injury Criteria for Pedestrian Safety, (2013) 14, 378–386

INTRODUCTION

The pedestrian is an extremely vulnerable road user, with thousands severely injured and killed around the world every year. In 2009, 19.5% of all fatalities (6711 victims) associated with road traffic accidents in the European Union were pedestrians, while the pedestrian fatalities of France accounted for 11.6% (ONSIR, 2010). The lower limbs in particular have been demonstrated in previous studies to be the most frequently injured body segment, accounting for approximately 1/3 of total pedestrian injuries (IHRA, 2001; Carter et al., 2008). In lower limb injury cases, knee injuries often lead to long-time treatment, even permanent impairment to the injured pedestrian (Liorzou, 1987).

To prevent knee injuries to pedestrians, one essential concern is to determine the injury tolerances of the corresponding parts by means of PMHS experimental tests or numerical simulations. Based on an in-depth investigation of real-world accidents, the International Harmonized Research Activities (IHRA, 2001) showed that 80-90% of pedestrians suffered lateral side impacts. Moreover, through experimental testing, several previous works have reported the injury tolerances of the knee joint considering the joint kinematics of pure lateral bending and shearing (Kajzer et al., 1990, 1993; Ramet et al., 1995). Regarding these test results, the injury criteria of European regulations were defined using isolated lateral bending (15 degrees) and shearing (6 mm) levels (EEVC, 1994; EEVC, 1998). However, consequent studies involving experimental testing and accident analysis (Kajzer et al. 1997; Kajzer et al. 1999; Teresinski and Madro 2001; Bose et al., 2004; Bose et al., 2008) revealed that knee joint injuries are correlated with combined lateral shearing and bending effects. Furthermore, Bose et al. (2008) explained that knee injuries are due to a varying combination of bending moments and shear forces, which are dependent on the location of loading relative to the knee joint center. Hence, the combined lateral bending and shearing contributions should be included in the knee injury criteria for pedestrian safety.

More recently, Bose et al. (2008) proposed an injury function combining lateral bending angle and shearing displacement for the medial collateral ligament (MCL) based on the isolated knee joint test design of Bose et al. (2004). The diverse data and method of regression indicated that the results depend strongly on the defined analysis for joint kinematics. Thus, the analysis would benefit from evaluation through corresponding experimental tests and FE simulations. MCL injuries were mostly recorded in the Bose et al. (2004) test series, and only one other injury of the anterior cruciate ligament (ACL) was reported as a slight laxity. However, knee joint injuries of the four major ligaments are not restricted to this isolated ligament injury, as indicated by the literature (Yasuhiro, 2005; Arnoux et al., 2006). The constrained knee kinematics (including knee flexion, axial torsion, anterior-posterior displacement) in these tests could limit injuries of other major ligaments. However, the knee is a 6-DOF joint without these constraints in real pedestrians. Moreover, experimental tests on an isolated anatomic segment can also be limited by the ability to monitor the kinematics of

internal tissues, for example, the ligament deformation of the knee joint in the global lower limb test. With the rapid development of computational power and numerical simulation, the finite element (FE) model with biofidelic properties has provided a valuable method to investigate the mechanical responses of different tissues or identify macroscopic local injuries by calculation, which cannot be recorded during experiments. Hence, coupling the advantages of both experiments and numerical simulations could be useful to investigate biomechanical issues.

Several FE models of lower limbs have been developed for investigating the detailed behaviors of anatomic structures (Bermond et al., 1994; Takahashi and Kikuchi 2000; Beillas et al., 2001; Untaroiu et al., 2005). Moreover, the corresponding methods for detecting knee joint injuries have also been proposed with element failure modeling, principally based on the ultimate strain level obtained directly from test results. However, this method may not be applicable for knee ligaments. Woo et al. (1983) found that the ultimate strain of a ligament substance was considerably lower than the specific deformation of the bone-ligament-bone complex. Based on tensile tests, Arnoux et al. (2002) also found that knee ligaments usually failed by the peeling or avulsion of the bone-ligament attachment. Therefore, these results indicate that the failure modeling of bone-ligament attachments could be critical for predicting ligament failure. Hence, the simple element failure modeling of ligament material can be considered incomplete. Recently, Arnoux et al. (2005) proposed a method to evaluate knee ligament injuries regarding the global deformation of ligaments by calculating the elongation of springs along ligament fiber axes, with the advantage of incorporating the ligament ultimate strain obtained from test results directly into simulation analysis.

The objective of the current study is to propose a knee injury criterion regarding possible initial knee joint failures by coupling the reported experimental results and the sensitivity analysis of the corresponding numerical simulations. The reported experimental tests attempted to replicate different injury mechanisms experienced by the pedestrian at various impact locations and to define incidences of injury to the knee joint. Following the experimental tests, an evaluated FE model was simulated by the sensitivity analysis of impact locations to calculate the accurate joint kinematics and develop a robust injury criterion for the knee joint. In consideration of the onset of knee injuries, the overall results of the dedicated sensitivity analysis indicate a new injury criterion for the knee joint by combining lateral bending and shearing mechanisms.

METHODS

Experimental Test

Seven isolated lower limbs tests with dynamic impact loadings were reported in the current study. All the post-mortem human subjects (PMHS) were obtained, treated and tested in accordance with the ethical guidelines established by the Ethical Committee of the Marseille Faculty of Medicine. As shown in Fig. 1, the experimental device was based on previous work conducted in our lab (Kajzer et al., 1990, 1993), with the main difference being the definition of the impactor interface. The dimensions of the impactor face reported in Kajzer et al.(1990, 1993) (150×50 mm) were changed to 150×100 mm in the current tests. In addition, the current test included two 3D accelerometers (Entran EGA, 250 g) screwed into the tibia

and two screwed into the femur. Thus, the occurrence of knee joint injury can be detected by the analysis of acceleration data. All selected subjects were examined via pre-crash X-ray imaging to exclude pathological variation and previous surgery on bone and joint structures. The lower limb was weight-bearing. Before the impact test, the lower extremity was dissected from the upper body. The specimens were preloaded with a mass of 40 kg to simulate the upper body mass of a human body (Fig.1.). Then, the thigh stability prior to the test was established by lower and upper thigh clamps, and an impactor loading mass of 37 kg was applied to the predetermined impact location. Fifty millimeter foam pads (Styrodur® C) were set in front of the plates of the thigh clamps and impactor. The impactor faces were equipped with force transducers (Sedeme, 20 kN). Furthermore, 3D accelerations from four Entran EGA (250 g) sensors on the tibia and femur were also collected to determine the exact failure time and occurrences of knee joint injury through signal analysis. Test data including impactor force and acceleration were sampled at 10000 Hz.

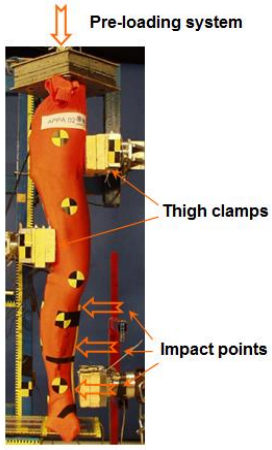

Fig. 1. Experimental apparatus with isolated lower limb subject

The relative height of a vehicle bumper in pedestrian anthropometry varies with bumper design and impact environment. The summary report of the International Harmonized Research Activities (IHRA) Pedestrian Safety Working Group provided insight into the impact velocity distribution associated with pedestrian impacts (2001). According to the analysis results, a large portion of pedestrian lower limb injuries were caused by impact velocities ranging from 20 km/h to 40 km/h. Furthermore, in previous studies (Kajzer et al., 1999; Masson et al., 2005), 20 km/h was typically used to represent the lower velocity for the isolated lower limb tests of pedestrian safety. Therefore, an initial velocity of 20 km/h was selected for the impactor in the current study. Considering the injury mechanisms of the knee joint relevant to those obtained by vehicle-pedestrian impact, the impactor was located at three locations on the tibia: the distal end to prioritize pure bending, the middle diaphysis to have a combined bending and shearing effect and the proximal end to acquire pure shearing. After the tests, the post necropsies of all specimens were performed by an orthopedic surgeon to examine the tissue injuries.

Finite Element Simulation

The “Lower Limb Model for Safety” (LLMS) model was used to analyze the structural responses of the lower limb (Fig. 2), which is a finite element model with detailed anatomy derived from a PMHS subject close to the 50th percentile human male. Its biofidelity has been

largely validated in the literature (Beillas et al., 2001,Arnoux et al., 2005,Bose et al., 2007,Mo et al., 2012). For the knee joint, Arnoux et al. (2005) and Masson et al. (2005) validated the LLMS model against the force thresholds of pure bending and shearing tests of Kajzer *et al.* (1990, 1993) and subsequent tests of Masson et al. (2005). Bose *et al.* (2007) evaluated the knee joint of this model by moment and ligament injury occurrences based on the isolated 4-point dynamic knee bending test from Bose et al. (2004).

Regarding the global strains of ligaments, the failure analysis method developed by Arnoux et al. (2005) was adopted to predict the occurrences of injury in the simulation. Arnoux et al. (2002) identified two failure modes of knee ligaments and classified them according to ligament type: cruciate ligaments (ACL and PCL) with peeling failure and cortical bone avulsion and collateral ligaments (MCL and Lateral collateral ligament- LCL) with bone avulsion from the attachment. Regarding the test results of Arnoux et al. (2002), a 24% ultimate strain for cruciate ligaments and 28% for collateral ligaments were determined to be the threshold of knee injury occurrence and were used to define injury in the simulation.

The FE model corresponding to the experimental test was set up as shown in Fig. 2. The model involved the use of thigh clamps to limit the movement of the thigh and pre-loading the system to model upper body weight and featured an impactor with foam pads. The FE simulation procedure was divided into two phases based on the experimental procedure. First, the thigh part was fixed by the clamps during the initial two milliseconds. Then, the leg was loaded by the impactor which was moving at an initial velocity of 20 km/h. Regarding the knee injury mechanisms of pure bending and pure shearing (corresponding to the distal and proximal impacts), the model validation has been previously reported in the literature (Arnoux et al. 2005, Masson et al. 2005). Therefore, the present study focused on the evaluation of model capabilities related to the knee injury mechanism of combined bending and shearing obtained with the impact on the tibia middle diaphysis. Based on the evaluated model, an in-depth sensitivity analysis by FE simulations was performed to develop a new injury criterion for the knee joint. Because the test results revealed the effects of impact locations on injury types and tolerances, twenty-four impact locations from the foot to the proximal tibia were defined for the sensitivity analysis, with an average interval of 14 mm. Both the injury mechanisms and tolerances of the knee joint were explored through kinematics analysis in the simulations.

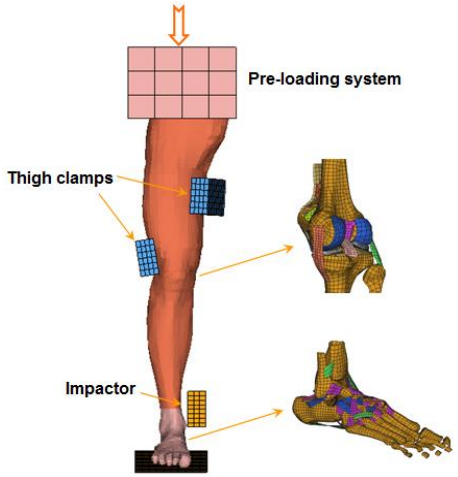

Fig. 2. FE model for modeling the experiments

The methods for recording lateral bending angle and lateral shear displacement are summarized in Fig. 3. The shear displacement was calculated by the relative distance of two points in the lateral direction. The bending angle was calculated from the angle of two vectors in the coronal plane, namely the lateral bending plane. Because the recording points were attached to the bone structures, the FE simulation excluded the influences related to the deformation of soft tissues relative to the experimental tests. Two measurement methods were employed for different purposes:

-The first method based on the experimental test, which is labeled with green vectors and points in Fig. 3. The vectors are along the tibia and femur diaphysial axes, based on the external markers stuck on the lower limb used in the test (Fig. 1.). In the middle of the knee joint, two points on the intercondylar eminence of the tibial plateau and the terminal groove of the femoral condyles were used to calculate shear displacement. Only the labeled points on the skin of test subjects can be used to analyze the bending angle using the video data. The shear displacement was also based on the relative displacement of the knee joint center. Thus, the classic method of performing shearing and bending measurements was chosen as Method 1 to compare the kinematics in the simulations with the test results.

-The second method was introduced to analyze the sensitivity of joint kinematics to knee injuries in the simulation and is depicted by red vectors and points in Fig. 3. It consisted of using the femur epicondyle axes as well as medial and lateral extremities of the tibia plateau to define vectors for analyzing the lateral bending in the coronal plane of the human body. Two corresponding points on the lateral tibial plateau and the lateral condyle of the femur were used to calculate lateral shearing by the relative displacement in the lateral direction. According to the coupling joint kinematics of bending and shearing, the measurement of shear displacement was also unavoidably influenced by lateral bending. However, the measurements of the pure shearing and pure bending of the joint kinematics were expected to serve as a basis for investigating the knee injury criteria. Therefore, the recording points for lateral shearing were located around the lateral bending center determined from joint kinematics to avoid this influence. In the present study, all lateral bending statements were related to the valgus rotation of knee joint. Thus, the nodes at the center of the lateral tibial plateau and the lateral condyle of femur were selected. These choices associated with calculating bending and shearing were made according to the analysis method introduced by Bose et al. (2008).

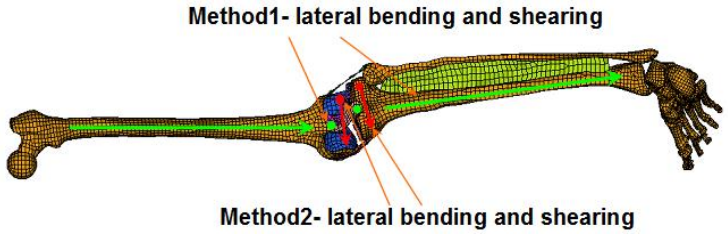

Fig. 3. Measuring methods of lateral bending and shearing

RESULTS

Experimental Test

The typical impact forces for the three impact locations are illustrated in Fig. 4. The force transducers mounted on the impactor face recorded these forces. The impact on the distal end of tibia exhibited one single peak with very brittle behavior. The impact on the middle diaphysis produced a typical force curve with two essentially different peaks. The impact force on the proximal end of the tibia presented ductile behavior with a continuously high level of force during the entire impact process.

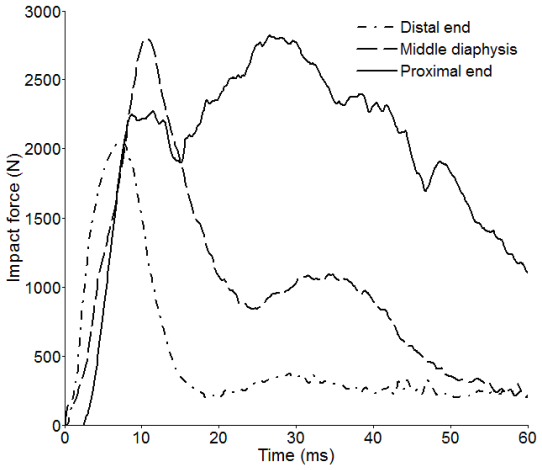

Fig. 4. The typical impact force curves on the three loading locations

The maximum impact forces in the lateral direction and the occurrence of knee joint injury in the experimental tests are summarized in Table 1. Both collateral and cruciate ligament failures were observed in the tests in addition to one case of bone fracture at the proximal-middle third junction of the fibula. Knee ligament bundles failed either at mid-ligament or at their bony attachments. The peak impact force was between 1884 N and 2817 N. In addition, Gabrielli (2010) also investigated the disturbance of acceleration data through signal analysis and estimated the possible failure times of initial knee injuries. Based on the defined injury onset from the acceleration data, the lower limb kinematics were analyzed by high-speed video to investigate the injury thresholds. In three tests (Dist1, Dist2, Mid3), there was non-injury or slight injury of the MCL. In these cases, these knee injuries cannot be distinguished clearly by signal analysis because of non-evident disturbances in the acceleration data. There were four tests in which the accelerometers recorded signals indicative of knee injury (Mid 1, Mid 2, Prox 1 and Prox 2). These tests are illustrated in Table 1 with the injury thresholds of lateral bending and shearing.

Table 1 Summary of experimental test results of lower limbs

Test Number	Age	Impact location	Max. Load (N)	Observed injuries	Bending (^{o})	Shearing mm
Dist1	92	Distal end	2042	MCL- Distal superficial injury	-	-
Dist2	99	Distal end	1884	None	-	-
Mid1	82	Middle diaphysis	2797	MCL- rupture at mid-substance below femoral insertion	21^{o}	8 mm
Mid2	79	Middle diaphysis	1870	MCL- avulsion at femoral level	18^{o}	10 mm
Mid3	81	Middle diaphysis	2074	MCL- slight laxity	-	-
Prox1	81	Proximal end	2666	MCL- avulsion at femoral insertion PCL- avulsion at femoral insertion ACL- avulsion at femoral insertion Fracture at the proximal-middle third junction of the fibula	12^{o}	22 mm
Prox2	82	Proximal end	2817	PCL- rupture at mid-substance LCL- Laxity at fibula head	12^{o}	19 mm

Notes: PCL represents posterior cruciate ligament;

LCL represents lateral collateral ligament;

"-" represents unknown values.

Finite Element Simulation

FE model evaluation

The evaluation of the FE model is reported for the middle diaphysis impact in the current study. The current tests validate the model for combined bending and shearing effects in addition to the previous validations for pure bending and shearing (Kajzer et al. 1990, 1993, Arnoux et al., 2005,Masson et al., 2005). The structural response of the biological subject was found to be largely related to the size and age of the subject. Because the size and age of subject Mid1 were close to the 50th cadaver subject used to develop the lower limb model, the results of the FE simulation were compared with these test results. The simulation results showed good correlation with the test results regarding the maximum force, stiffness and overall kinematics (Fig. 5 to 7).

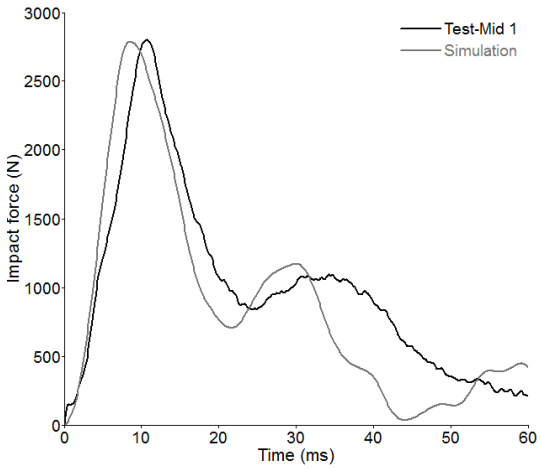

Fig. 5. Impact force-time history of the FE simulation and experimental test

The method for locating the failure tolerance of ligaments in the simulation was performed as follows. First, in Fig. 6, the global strains of the knee ligament showed that the MCL elongated until reaching the 28% strain threshold level 28 ms after impact. Then, based on the failure time (28 ms) identified in the previous step, the failure occurrences were acquired on lateral bending and shearing versus time curves (Fig. 7). A comparison of the test results showed that the MCL failure properties with both bending angles (16º by Method 1 and 14º by Method 2) and shear displacements (10 mm by Method 1 and 7 mm by Method 2) correlated well with the experimental results performed on the middle diaphysis of the tibia in Table 1. The lateral bending curve calculated from the two methods showed similar trends with different fluctuations in the middle parts (Fig. 7). In addition, unreported secondary PCL failure (33 ms) was also noticed in the simulation (Fig. 6).

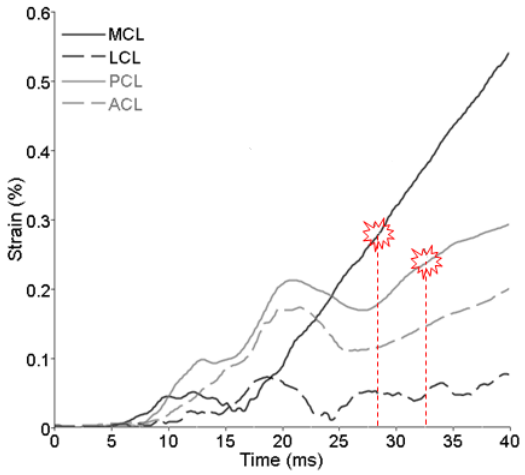

Fig. 6. Global strain of knee ligaments in the FE simulation

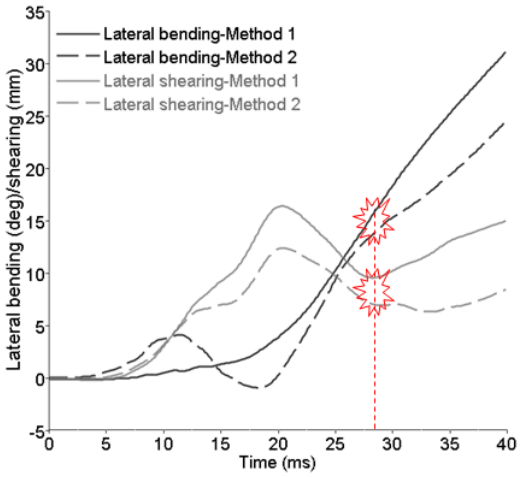

Fig. 7. Lateral bending angle and shear displacement in the FE simulation

Sensitivity analysis of impact locations

A sensitivity analysis relevant to impact locations was carried out to investigate the injury mechanisms as well as injury tolerances of the knee joint. The injury occurrences of the initial knee injuries to the impact locations are shown in Fig. 8 (zero height corresponding to lowest foot impact). Both MCL and cruciate ligament injuries were observed to be the first knee injuries, while the MCL was the most frequently injured part. The overall results indicate that the initial knee failures of cruciate ligaments were mostly caused by the impacts close to the proximal end of tibia where there is a large shear displacement. In contrast, the initial MCL failures were mainly caused by the impacts below the tibia mid-shaft, with large lateral bending levels.

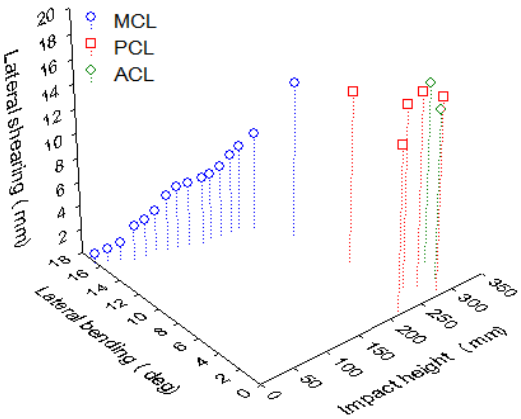

Fig. 8. The influence of impact location on the kinematic thresholds of initial knee injuries

Therefore, regarding the injury mechanisms of different failure patterns, the recommended injury criterion of the knee joint is composed of two thresholds: the isolated shearing threshold for cruciate ligament failure and the combined bending and shearing function for MCL injuries. The shearing threshold was the average level calculated from the shear displacements of initial cruciate ligament injuries. To consider the robustness and exactness of the developed MCL injury function, both initial and ensuing injury occurrences of the MCL were included in the quadratic regression (Fig. 9, Table 2). The threshold curve developed from the injury threshold function determined by the regression analysis of the experimental

failure data in the Bose et al. (2008) study is also presented in Fig. 9 for comparison with the current results. It was noticed that the limits of lateral bending and shearing in the current study are well correlated with those reported in the Bose et al. (2008) study. The contour of the injury function is different.

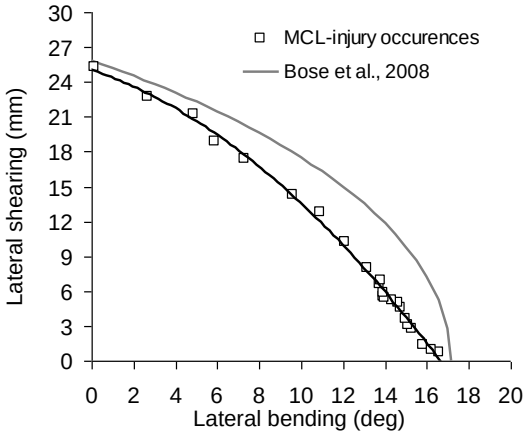

Fig. 9. Development of regressive function of MCL injury occurrences

Figure 10 presents an injury criterion of the whole knee joint by assembling the injury risk of all knee ligaments related to the onset of knee injuries. The new injury criterion combines MCL failure related to the onset of knee injuries from Fig. 9 with a bending level above 9 degrees in the regressive curve. Above 9 degrees, the cruciate ligaments are only secondary injuries. On the other hand, below this level, the onset of knee injury is related to cruciate ligaments with an isolated shearing threshold (Fig. 10, Table 2). However, this also means that when the bending angle is below 9 degrees, the MCL could suffer a potential secondary injury following the primary knee injury of the cruciate ligaments.

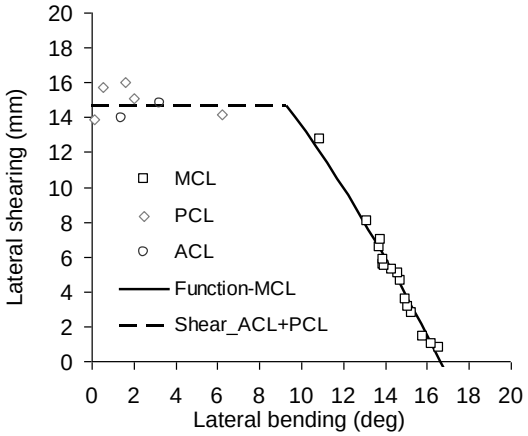

Fig. 10. Knee injury criterion categorized by initial injury types

Table 2. Descriptions of the knee injury criterion

Injury types	Injury criterion of knee joint
MCL	$D_{shearing} = -0.054B_{bending}^{\ 2} - 0.62B_{bending} + 25$ ($R^2 = 0.99$, $B_{bending} \geq 9^\circ$)
Cruciate ligaments	$D_{shearing} = 15\,\text{mm}$ ($0^\circ \leq B_{bending} \leq 9^\circ$)

Notes: $D_{shearing}$ represents lateral shear displacement and $B_{bending}$ is lateral bending angle.

DISCUSSION

Understanding knee joint kinematics and injury tolerances under vehicle-pedestrian loading is essential to creating countermeasures that can mitigate the severity of injuries to the lower limbs. The present study combined experimental tests and finite element simulations to investigate the injury criteria of the knee joint for pedestrian safety, considering the kinematics of the knee joint with combined lateral bending and shearing mechanisms. The overall test results reported in the literature suggest that the knee joint suffers from both ligament injuries and bone fractures. A high incidence of MCL failure was observed in the reported tests, while the MCL has also been indicated as the most easily injured ligament in real-world road accidents (Teresinski and Madro 2001). Other ligament injuries were also reported, especially for impacts close to the knee joint. Furthermore, evidence of combined bending and shearing effects reported in real vehicle-pedestrian accidents was also obtained from video analysis and the failures reported in Table 1 when impacts occurred at different locations. Both knee failures and kinematics indicated that the injury mechanisms of the knee joint in the currently reported experimental tests were relevant to vehicle-pedestrian impacts.

The recorded impact forces in the shear direction showed different features according to the relative impact locations (Fig. 4). The kinetic energy of the impactor was principally transferred by bending moment and shear force. While bending moments were not recorded in the tests, it is evident that the higher-force impact resulting from the energy release and blocking of the lower thigh clamp corresponds to a higher shear level. Therefore, these differences also confirm multiple modes of injury mechanisms of the knee joint. The distal end impact was close to pure bending, the proximal end impact was approximated as pure shearing loading and the middle diaphysis produced combined bending and shearing. Then, it can be concluded that the contributions of bending moment and shear force are essentially influenced by impact location. This phenomenon also demonstrates that isolated bending moment or shear force cannot be used as the sole injury tolerances of the knee joint. While the impact forces of the test results showed different features, the knee injury types and their severity seemed to also be related to impact location. As shown in Table 1, distal and middle tibia impact showed isolated MCL failures, while complex collateral and cruciate ligament injuries were observed to have resulted from proximal tibia impacts. The MCL was always considered the primary restraint to valgus rotation, namely lateral bending, in the current study. The cruciate ligaments were usually described as the primary restraint to tibia anterior/posterior translation and the secondary restraint to valgus/varus rotation (Goldblatt

and Richmond 2003). Considering the failure occurrences of the cruciate ligament under proximal impact (pure shearing), cruciate ligaments can also be assumed to have an important contribution to restraining lateral shearing (tibia lateral translation in the current study).

Note that there are several drawbacks in the design of the experimental work. First, bone mineral density (or BMD) was not measured in subjects as an indirect indicator of osteoporosis and bone fracture risk. Most injuries were the ligament avulsions related to ligament-bone insertion failures, which indicate that BMD measurement may be useful in better understanding these injury mechanisms. Second, the impacting load cell was not inertially compensated. To obtain better force data, this issue should be resolved in future works. On the other hand, the goal of the current study was not to provide reference force data by experiment but to build an injury criterion of knee joints with coupling experiments and simulations. The experimental results were principally used to strengthen the model's reliability and provide insight into injury occurrences related to loading conditions (including injury mechanisms and types). This means that the definition of the current injury criteria was not influenced by testing parameters such as BMD or compensated force. Third, in the current study, the lower limb was pre-loaded with a mass of 40 kg close to the upper body or half body's weight of the 50^{th} percentile human male. In the design of a pedestrian test system, Kam et al. (2005) summarized the results of previous studies and indicated that double support (both lower limbs in contact with the ground) account for 16-22% of a full gait cycle. However, this does not mean that both lower limbs support an equal amount of weight in this stance phase. The single foot support accounts for a larger percentage of the gait cycle. Further simulations performed in our lab showed that the pre-loaded weight does not have a significant influence on the force results, especially for the first peak level. However, the influence of pre-loading weight on the experiments could still be interesting for future study, although the impact is limited over very short times.

Although macroscopic injuries could be found through dissection, the initial failure time of the knee joint was hardly determined by the camera or other test data due to the complex kinematics of the knee joint and surrounding muscle tissues. Signal analysis of the acceleration data was conducted to determine the initial injury time of the knee joint, followed by the calculation of the corresponding injury thresholds from video analysis. The signal analysis reported by Gabrielli (2010) indicated the possible failure time of initial knee injuries without delineating clear failure types, accompanied by the signal disturbance in the acceleration data. However, once the exact failure time was determined, the accuracy of the bending tolerance acquired by rapid cinematograph analysis could also be limited by the deformation of soft tissues and difficulties in accurately determining kinematics from high-speed camera data. From an experimental point of view, the potential variation could be induced by the deformation of surrounding soft tissues and the numerical high-speed camera resolution, approximated to 3-4° degrees in the bending calculation. Hence, these data demonstrate the importance of the application of the FE simulation to investigate accurate joint kinematics through marking points on bones.

A biofidelic FE lower limb model was used to simulate the reported experiments and to predict accurate joint kinematics. In this section of the study, the FE model and its corresponding failure analysis methods were first evaluated against the test results. Good correlations between impact force and injury tolerance were found. As described before, two methods of measuring joint kinematics were employed in the current study. For bending

measurements, if the vectors were maintained in the lateral bending plane (coronal plane of human body), the two methods would give almost the same results regarding the mathematical theory. However, the knee joint kinematics of a pedestrian could be composed of lateral bending, lateral shearing, tibia axial rotation, etc. Despite the non-significant levels of these other kinematics, these joint kinematics complicated the measurement of lateral bending when calculating the bending angle in the 2D coronal plane by the projection of the spatial vector position. Thus, the results obtained from these two methods may present differences (Fig. 7). For shearing measurements, as described before, lateral shearing values may have been unavoidably influenced by bending levels unless the measuring nodes were located in the lateral bending center. This phenomenon was indicated by the higher level of lateral shearing recorded by Method 1 when compared with Method 2 (Fig. 7.). In the current study, lateral bending in all cases were related to the valgus rotation of the knee joint; thus, the nodes of Method 2 were chosen on the center of the lateral femoral condyle and the lateral tibial plateau. Nevertheless, in the case of varus rotation, the nodes on the center of the medial femoral condyle and the medial tibial plateau should be used. Compared with Method 1, a more significant influence of lateral bending and lateral shear displacement can be noticed from the overall time history from the results of Method 2 (Fig. 7). Furthermore, the correlation between the two bending calculation methods could be investigated in the future to define the correction factors associated with classical bending measurements in the experimental tests.

In addition, although the LLMS model provided a good prediction of initial knee joint injuries compared with the test results, the secondary injury of PCL failure recorded in the simulation was not reported in the corresponding test (Fig. 6). This potential occurrence was also discussed in previous studies (Arnoux et al., 2005; Bose et al., 2007). There are two possible reasons for this. First, because the failure threshold of global strain was used to predict knee joint injuries, failure modeling at element levels was not part of the model. This means that the model could not predict secondary injuries of the knee joint as exactly as it can predict initial injuries. Second, because non-homogenous strain distributions considering local strain levels were presented along the ligaments due to the joint kinematics and bone-ligament attachments, the combination of global and local strain could be a more viable method for failure evaluation. Moreover, the failure modeling of knee ligaments and relevant bone structures around attachments could be included in the FE model directly in the future to better predict the occurrences of initial and the following knee injuries for the avulsion or rupture of knee ligaments.

Because impact location was indicated to be a key factor influencing knee joint injuries in the experimental tests, a sensitivity analysis of impact location by FE simulation was implemented to evaluate the robustness of the injury criteria. The results of these simulations show the overall initial knee failures in Fig. 8 and indicate that the impact height could dominate the type of initial joint injuries sustained and the corresponding shearing and bending tolerances. The incremental increase in height revealed that the failure tolerances exhibited a tendency to increase the shearing levels and decrease the bending levels. It was also demonstrated that MCL, PCL, and ACL could all be initial knee injuries. MCL was the most frequently injured part in the simulations as well as in the tests, caused by the lower height impacts usually associated with a high level of lateral bending. Initial injuries of the cruciate ligaments were mostly caused by the impacts close to knee joints. Thus, it appears that shearing level dominates cruciate ligament failure, as indicated by the tests, while

combined valgus bending and lateral shearing is responsible for MCL failure.

Hence, based on the analysis above, the new injury criterion for the pedestrian knee joint is categorized as biphasic: a combined bending and shearing function for MCL injuries and a dominant lateral shearing threshold for cruciate ligaments. As a result, the new injury criterion for initial knee joint injuries is defined as follows (Table 2): an average shearing threshold (15 mm) for initial cruciate ligament failures and a combined injury function of bending and shearing levels (started from 9 degrees to 17 degrees) for MCL injuries. In the development of an injury function for isolated MCL injuries, it should be noted that the injury functions developed by the sensitivity analysis of FE simulations ultimately agree with the definition of the injury function of Bose et al. (2008) study based on the experimental tests (Fig. 9). The agreement with the injury function of Bose et al. (2008) also validates the efficiency of the injury function for MCL injuries in the current study. On the other hand, the potential differences in the curve shapes could be attributed to the different boundary conditions and analysis methods used. In the Bose et al. (2008) study, isolated MCL injuries (only one ACL laxity) were found. This could be due to the constraints of experimental boundary conditions on the knee joint. In the current study, the knee was set as free without limitations to joint kinematics. In this case, multiple knee injuries were found in the FE simulations as well as in the experimental tests. Considering initial knee injuries, there were also different injury types occurring at the first injury, including ACL, PCL and MCL, due to various loading conditions. Therefore, regarding knee joint kinematics, the combined injury criterion separated by initial knee injury types, including cruciate ligaments and MCL injuries, is proposed in the current study as shown in Fig. 10. All the impacts in the simulations and experimental tests were located below the center of the knee joint. This induced only lateral shearing with tibia lateral translation and lateral bending with valgus rotation, which were the only loading conditions considered in the current study. However, regarding the relative height of a vehicle bumper to the height of the knee joint, knee joint injuries under lateral impact could also be caused by tibia medial translation and varus rotation. Because LCL presents a primary restraint to varus bending (Weiss, Gardiner 2001), initial LCL injury tolerances could also be included in the new injury criterion, while considering the impact of varus bending dominance. Thus, whether tibia lateral and medial translation during lateral shearing, valgus and varus rotation during lateral bending have the same threshold levels or not regarding the asymmetric interior structure of knee joint should be determined in the future.

In addition, we focused on the experimental test and FE simulation of the sub-segment of the human body. The testing condition of the present study is not real world car-pedestrian impact condition. Because most previous isolated sub-segment tests for the knee injuries of pedestrians were related to the pure bending and shearing mechanisms (Kajzer *et al.* 1990, 1993, Kajzer *et al.* 1997, Kajzer *et al.* 1999), the principal consideration for using the current test configuration is to reflect combined lateral bending and shearing mechanisms with various loading locations. We noted that the variation of injury types and thresholds with impact locations and established the injury criterion by the sensitive analysis of impact locations with FE simulations. In the future, full-scale pedestrian testing and simulations should be conducted to better understand the robustness and availability of the current injury criterion, considering the influence of the entire vehicle front-end shape and properties.

REFERENCES

Arnoux PJ, Cavallero C, Chabrand P, Brunet C. Knee ligament failure under dynamic loadings. *Int. J. Crashworthiness.* 2002;7:255-268.

Arnoux PJ, Cesari D, Behr M, Thollon L, Brunet C. Pedestrian lower limb injury criteria evaluation: A finite element approach. *Traffic Inj. Prev.* 2005;6:288-297.

Arnoux PJ, Thollon L, Behr M, Brunet C, Cesari D. Knee joint injury mechanisms and injury criteria in full scale tests according to impact position. In: *Proceedings of the 2006 International Research Council on Biomechanics of Injury (IRCOBI) Conference, Madrid, Spain, 2006*: 319-322.

Beillas P, Begeman PC, Yang KH, King AI, Arnoux PJ, Kang HS, Kayvantash K, Brunet C, Cavallero C, Prasad P. Lower limb: Advanced fe model and new experimental data. *Stapp Car Crash J.* 2001;45:469-494.

Bermond F, Ramet M, Bouquet R, Cesari D. A finite element model of the pedestrian knee-joint in lateral impct. In: *Proceedings of the 1994 International Conference on the Biomechanics Impacts (IRCOBI), Bron, France,1994*: 117-129.

Bose D, Arnoux PJ, Cardot J, Brunet C. Evaluation of knee injury threshold in pedestrian-car crash loading using numerical approach. *Int. J. Crashworthiness.* 2007;12:381-399.

Bose D, Bhalla K, Rooij L, Millington S, Studley A, Crandall J. Response of the knee joint to the pedestrian impact loading environment. *SAE Technical Paper 2004-01-1608.* 2004; doi:10.4271/2004-01-1608.

Bose D, Bhalla KS, Untaroiu CD, Ivarsson BJ, Crandall JR, Hurwitz S. Injury tolerance and moment response of the knee joint to combined valgus bending and shear loading. *J. Biomech. Eng.-Trans. ASME.* 2008;130: 031008-1-8.

Carter EL, Neal-Sturgess CE, Hardy RN. Aprosys in-depth database of serious pedestrian and cyclist impacts with vehicles. *Int. J. Crashworthiness.* 2008;13:629-642.

Gabrielli F. *Apport des techniques temps frequence a la caracterisation mecanique du corps humain en choc.* [Ph.D. thesis]. Marseille, Université de la Méditerranée; 2010.

Goldblatt JP, Richmond JC. Anatomy and biomechanics of the knee. *Operative Techniques in Sports Medicine.* 2003;11:172-186.

International Harmonized Research Activities (IHRA). *Pedestrian safety working group 2001 report.* 2001.

Kajzer J, Cavallero C, Bonnoit J, Morjane A, Ghanouchi.S. Response of the knee joint in lateral impact: Effect of shearing loads. In: *Proceedings of the 1990 International Research Council on Biomechanics of Injury (IRCOBI) Conference, Bron, France, 1990*: 293-304.

Kajzer J, Cavallero C, Bonnoit J, Morjane A, Ghanouchi.S. Response of the knee joint in lateral impact: Effect of bending loads. In: *Proceedings of the 1993 International Research Council on Biomechanics of Injury (IRCOBI) Conference, Eindhoven, The Netherlands, 1993*: 105-116.

Kajzer J, Matsui Y, Ishikawa H, Schroeder G. Shearing and bending effects at the knee joint at low speed lateral loading. *SAE Technical Paper 1999-01-0712.* 1999, doi:10.4271/1999-01-0712.

Kajzer J, Schroeder G, Ishikawa H, Matsui Y. Shearing and bending effects at the knee joint at high speed lateral loading. *SAE Technical Paper 973326.* 1997; doi:10.4271/973326.

Kam, CY, Kerrigan, J, Meissner, M, Drinkwater, C, Murphy, D, Bolton, J, Arregui, C, Kendall, R, Ivarsson, J, Crandall, J, Deng, B, Wang, JT, Kerkeling, C, Hahn, W. Design of a full-scale impact system for analysis of vehicle pedestrian collisions. *SAE Technical Paper 2005-01-1875.* 2005; doi:10.4271/2005-01-1875.

Liorzou G. *Le genou ligamentaire: Examen clinique.* Springer-Verlag; 1987.

Masson C, Arnoux PJ, Brunet C, Cesari D. Pedestrian injury mechanisms & criteria: A coupled experimental and finite element approach. In: *Proceedings of the 19th International Technical Conference on the Enhanced Safety of Vehicles Conference (ESV), Lyon, France, 2005*: Paper No. 05-0335.

Mo F, Arnoux PJ, Jure JJ, Masson C. Injury tolerance of tibia for the car–pedestrian impact. *Accident Analysis & Prevention.* 2012;46:18-25.

Obervatoire National Interministériel de la Sécurité Routière. *La sécurité routière en france: Bilan de*

l'année 2010. 2010.
European Experimental Vehicles Committee: Working Group 10 on Pedestrian Proctection (EEVC/WG10). *Proposals for methods to evaluate pedestrian protection for passenger cars: Final report.* 1994.
European Experimental Vehicles Committee: Working Group 17 on Pedestrian Proctection (EEVC/WG17). *Improved test methods to evaluate pedestrian protection afforded by passenger cars.* 1998.
Ramet M, Bouquet R, Bermond F, Caire Y. Shearing and bending effects at the knee joint tests in quasi-static lateral load. In: *Proceedings of the 1995 International Research Council on Biomechanics of Injury (IRCOBI) Conference, Brunnen, Switzerland, 1995*: 93-105.
Takahashi Y, Kikuchi Y. Development and validation of the finite element models for the human lower limb of pedestrians. In: *Proceedings of the 44th Stapp Car Crash Conference, Atlanta, Georgia, USA, 2000*; Paper No. 2000-01-SC22.
Teresinski G, Madro R. Knee joint injuries as a reconstructive factors in car-to-pedestrian accidents. *Forensic Sci.Int.* 2001;124:74-82.
Untaroiu C, Darvish K, Crandall J, Deng B, Wang JT. A finite element model of the lower limb for simulating pedestrian impacts. *Stapp Car Crash Journal.* 2005;49:157-181.
Weiss JA, Gardiner JC. Computational modeling of ligament mechanics. *Crit. Rev. Biomed. Eng.* 2001;29:303-371.
Yasuhiro M. Effects of vehicle bumper height and impact velocity on type of lower extremity injury in vehicle–pedestrian accidents. *Accident Analysis & Prevention.* 2005;37:633-640.

III. Investigation of the injury threshold of knee ligaments by the parametric study of car-pedestrian impact conditions

This article is published in Safety Science : Mo F, Arnoux PJ, Cesari D, Masson C. Investigation of the injury threshold of knee ligaments by the parametric study of car-pedestrian impact conditions. Safety Science. 62, 2014, 58–67

INTRODUCTION

Traffic injury is a worldwide safety problem; the fatalities in traffic crashes each year are estimated at almost 1.2 million, while the injured could reach as high as 50 millions (Peten et al., 2004). Among the deaths, the majority are currently the "vulnerable road users": pedestrians, pedal cyclists and motorcyclists. The pedestrian is the most vulnerable road user, who represents 12.1% of road crash victim fatalities according to 2010 accident data in France (Obervatoire National Interministériel de la Sécurité Routière [National interministerial Road Safety], 2011). Lower limbs were the most commonly injured body segment, accounting for about one third of the AIS (Abbreviated Injury Scale) 2-6 pedestrian injuries (Cater et al., 2008; International Harmonized Research Activities (IHRA), 2001). The IHRA (2001) data also showed that the bumper is the leading source for pedestrian lower limb injuries.

Car improvement guidelines for pedestrian safety are closely related to assessments reflecting real world accidents. The European Union Directive 2003/102/EC (2003) enacted the first legislation to protect pedestrians and other vulnerable road users when in collision with a passenger car, and introduced test requirements for vehicles based on the research of the European Experimental Vehicles Committee Work Groups (1994; 1998). A lateral bending anlge of 15 degrees and a lateral shear displacement of 6 mm are proposed as the thresholds for knee injuries in the test requirements in particular for the rupture of knee ligaments. In this case, the bending angle threshold was associated with the bending moment at knee level, while the lateral shearing threshold of 6mm was based on a shear force in cadaver experiments. After the works of the EEVC/WG10 (1994), many studies investigated the injury threshold of the knee joint by considering lateral shearing and bending values using contrived isolated sub-segment loading experiments. Quasi-static lateral shearing and bending test results from Ramet et al. (1995) showed that the first microscopic injury of the ligaments appeared above 12 mm of lateral shearing, while the first macroscopic lesion appeared above 16 degrees of lateral bending. However, EEVC/WG17 indicated that non-preloaded knee joints in the tests could influence the results. Then Kajzer et al. (1999; 1997) conducted isolated lower limb tests exposed to lateral shearing and bending at a high velocity (40km/h), and at a lower velocity (20km/h). The thresholds of lateral shear displacement and bending angle (16 mm and 12.3 degrees) for the initial damage of the ligaments at the low speed were found to be similar to those at high-speed lateral loading (16 mm and 14.6 degrees). Kerrigan et al. (2003) conducted two lateral shearing tests and three lateral bending tests with isolated knee joints using acoustic sensors, to monitor the primary injury occurrence of the ligaments. Based on the results of Kerrigan et al. (2003), Bhalla et al. (2003) summarized that anterior cruciate ligament (ACL) failures occurred at shear displacements of 12.7 and 17.8 mm in two shearing tests, while the medial collateral ligament (MCL) failed at approximately 12.7 degrees in three bending tests. However, these previous thresholds all considered bending and shearing values separately, and only used the data from isolated sub-segment tests.

Recently, Arnoux et al. (2006) indicated that knee ligament injuries could be attributed to the combined effects of shearing and bending, which vary with the relative impact height of the lower extremity to the car bumper. Bose et al. (2008) defined an injury threshold function for the MCL that combined lateral bending angle and lateral shear displacement by the regression of experimental data derived from isolated knee joint tests. However, the experimental data show large variation and other knee ligament injury types were also not included in this threshold various failure types function, such as the failure of cruciate ligaments noted in pedestrian accidents and full-scale vehicle-pedestrian experiments (Kerrigan et al., 2008; Masson et al., 2007; Teresinski and Madro, 2001). Furthermore, based on isolated lower limb tests and the corresponding sensitive analysis of finite element (FE) simulations, Mo et al. (2012c) proposed injury criteria with combined bending and shearing contributions, by considering various failure types of initial knee ligament injuries (including cruciate ligaments and the MCL). Because the loading condition of the lower limbs in this study was artificially designed for sub-segment experimental tests, the entire shape of the car front-end was still not included in simulating the real car-pedestrian impact. The efficiency of these injury criteria still needs to be evaluated in realistic car-pedestrian impact conditions.

Hence, the current study aims to investigate knee ligament injury thresholds in car-pedestrian impact environments as well as to evaluate the previous injury criteria proposed by isolated sub-segment tests. A parametric study of various pedestrian loading conditions was implemented. Three impact factors were considered: impact heights, locations of impact and impact velocities. Initial injury occurrences of both cruciate ligaments and MCLs were found, and were used to develop injury thresholds correlated with combined knee joint kinematics.

MATERIAL AND METHODS

Car-pedestrian impact model

The parametric study of FE simulations is focused on a biofidelic finite element model of the lower limb – the “Lower Limb Model for Safety” (LLMS) based on Radioss codes, which has been validated in a series of experimental tests ranging from isolated tissue tests to whole limb impacts, as shown in Table A.1 (Arnoux et al., 2005; Beillas et al., 2001; Bose et al., 2007; Masson et al., 2005; Mo et al., 2012a; Mo et al., 2012c). The model geometry was derived from MRI (Magnetic resonance imaging) measurements of a subject close to the 50th percentile human male, including detailed anatomic structures of a lower limb from the hip joint to the toe region (Fig. A.1). The modeling of compact and spongy bone materials used a Johnson Cook elastoplastic material law, as shown in Table A.2. Knee ligaments were modeled using a generalized viscoelastic material (Kelvin Voigt law) as shown in Table A.3. The contact between bones, ligaments and cartilages was modeled with multipurpose contacts by defining alterative master surface and edge-to-edge contacts. The pedestrian model was the combination of the 50% Hybrid-III dummy model and the LLMS model at the hip joint, in order to include the entire human body mass and inertial effects (Fig. 1). A new- generation car model was included to simulate realistic car-pedestrian impacts in the lateral impact direction. The entire car-pedestrian impact model has been evaluated in regards to pedestrian lower limb kinematics in the previous study (Mo et al., 2012b).

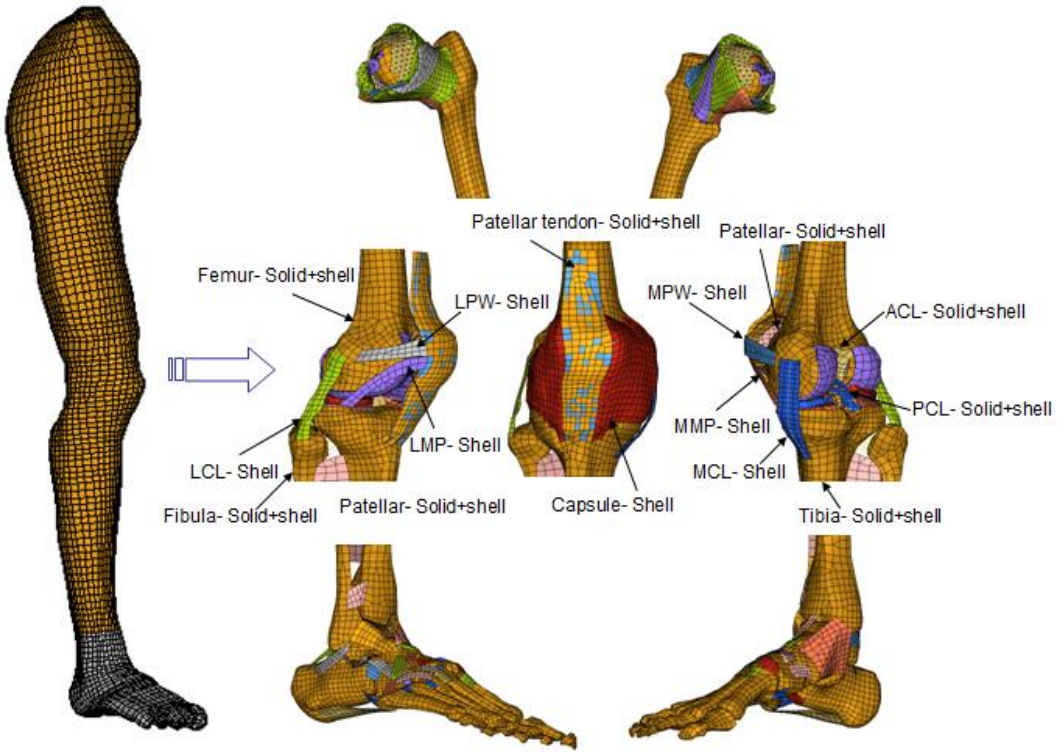

Figure A.1 Overview of "Lower Limb Model for Safety": medial and lateral collateral ligament (MCL and LCL); anterior and posterior cruciate ligament (ACL and PCL); medial and lateral patellar wing (MPW and LPW); medial and lateral meniscus patellar ligament (MMP and LMP).

Table A.1 Summary of the validations of the LLMS model (Arnoux et al., 2005; Beillas et al., 2001; Bose et al., 2007; Masson et al., 2005; Mo et al., 2012a; Mo et al., 2012c).

	Validation experiments	Experimental references	Parameters
Isolated Tissues	Ligament bone complex traction	Arnoux (2000)	Force, displacement
	Quasi-static three-point bending of tibia and femur	Jundt (2007)	Force, displacement
	Dynamic three-point bending of femur	Beillas (1999)	Force, displacement
Sub-segment loading	Dynamic three-point bending of leg	Nyquist et al. (1985)	Moment
	Patellar impact on flexed knee	Haut and Atkinson (1995) and Hayashi et al.(1996)	Force, time
	Tibia impact on flexed knee	Banglmaier et al. (1999)	Force, time
	Anterior-posterior flexed knee	Viano et al. (1978)	Force, displacement
	Knee lateral-medial bending/ combined loading	Bose et al. (2007; 2004; 2008)	Moment, injury occurrences
Whole lower limb tests	Quasi-static lateral shearing/bending	Ramet et al. (1995)	Force, shear displacement/bending angle
	Dynamic lateral shearing/bending	Kajzer et al. (1990, 1993)	Force, shear displacement/bending angle
	Dynamic combined lateral shearing and bending	Mo et al. (2012c)	Force, shear displacement/bending angle

	Frontal sled test	Beillas et al. (2001)	Force, time

Table A.2 Summary of elastoplastic properties of bones.

	Density (g/mm^3)	Young's Modulus (MPa)	Poisson's ratio	Yield Stress (MPa)	Ultimate strain	Ultimate Stress (MPa)
Compact bone	0.0015-0.0021	9000-15000	0.3	80- 120	2- 3	110- 130
Spongy bones	0.0013-0.00185	10- 450	0.3	10	3	15

Arnoux et al. (2002) indicated that collateral ligaments exhibit a different failure mode than cruciate ligaments. Based on this difference, the authors summarized that the ultimate strain of cruciate ligaments is between 18% and 24% while that of collateral ligaments is between 25% and 38%. Given the tendency of the experimental test results, a 24% strain level for cruciate ligaments and 28% strain level for collateral ligaments were defined as thresholds to predict ligament failures in the model. We measure ligament strain by means of several low stiffness springs attached to the elements of these ligaments. These sensors were defined along the main fiber axis on the middle line of the ligaments. Consequently, we can investigate local deformation as well as global deformation of the ligaments by recording the spring elongation in the simulation. In the current study, if the global strain (the engineering strain of the entire ligament) of one ligament reaches its defined strain threshold, we suppose this ligament fails at this moment. Using this method, the LLMS model has shown its ability to provide good assessments of knee ligament injuries under complex loading conditions (Arnoux et al. 2005; Bose et al. 2007).

According to this definition of ligament failure, the injury threshold would be developed by correlating the injury occurrences of the ligaments to joint kinematics. The literature described the knee joint as having six physical moving modes (Grood and Suntay, 1983; Weiss and Gardiner, 2001), including anterior-posterior, medial-lateral and distal-proximal translations as well as flexion-extension, internal-external and varus-valgus rotations. One challenge is to define the way to properly record knee joint global kinematics during simulations. Regarding the relative movement of the tibia to the femur, knee lateral translation can be approached by two methods: lateral movement of the tibia to femur, and medial movement of the femur to tibia. To distinguish the direction, we take the femur as the reference and define the moving direction of the knee by the relative movement of the tibia to the femur in the current study (e.g., the distal-proximal translation of the knee was defined as two groups: tibia distal translation and tibia proximal translation). Other knee impact responses also added "tibia" in front of them to indicate moving directions. In the car-pedestrian impact, lateral bending represents varus/valgus rotation, while lateral shearing represents medial/lateral translation. Regarding the dominant pedestrian knee injury mechanisms, the combined contribution of lateral bending and shearing was analyzed in the current study. Other joint kinematics with evident influences on this combined contribution to ligament injuries were also discussed, such as tibia distal/proximal translation and tibia

internal/external rotation.

Table A.3 Summary of viscoelastic properties of knee ligaments.

	LCL	MCL	PCL	ACL
Yong's modulus (MPa)	50	60	120	70
Poisson ratio	0.3	0.3	0.3	0.3
Tangent Young's modulus (MPa)	48	58	105	65
Viscosity coef. (pure shear)	6.6	6.6	6.6	6.6

Figure 2 shows the methods for measuring knee joint kinematic responses. Lateral bending and tibia internal/external rotation are calculated from two vectors, as shown in Figure 2. They are defined on femur epicondyle axes as well as medial and lateral extremities of the tibial plateau. Lateral bending was obtained from a varying angle of two vectors in the coronal plane of the human body. Tibia internal/external rotation was the value of two vectors in the transverse plane. Two points (Point 1 and 3) on the lateral tibial plateau and the lateral femoral condyle are used to calculate lateral shearing and tibia distal/proximal translation by their relative displacement in the lateral direction and axial direction, respectively.

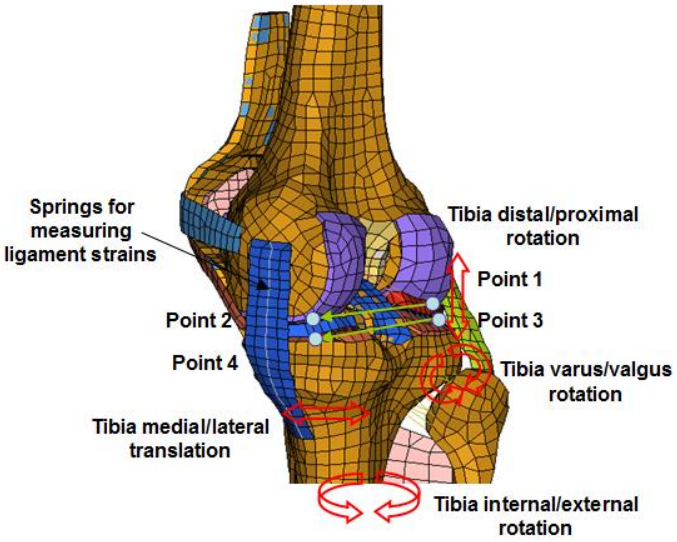

Fig. 2. Measurement of the responses of knee joint kinematics.

Parametric study

Regarding various car-pedestrian impact enviroments, three factors were considered in the parametric study: impact velocities, locations and heights. The summary report of the International Harmonized Research Activities (IHRA) Pedestrian Safety Working Group provided insight into the impact velocity distribution associated with pedestrian accidents (IHRA 2001). Based on this analysis, three levels (20 km/h, 30km/h and 40 km/h) were selected in the parametric study.

In the design of a car front-end structure for pedestrian protection, there are usually three characteristics that need to be considered: sufficient crush depth, appropriate deformation stiffness, and appropriate force distribution. To consider the influence of combinations of shape and stiffness, three contrastive impact locations were selected as follows:

- P01 is in front of the crash can and longitudinal beam. This zone is the rigid region theoretically;
- P03 is in the middle of the bumper. This zone is the flexible region theoretically;
- P02 is in the middle of P01 and P03, around the headlight corner.

Figure 3 shows the contours (also including bumper sections) of two impact locations of the car: in front of the crash can (P01) and in front of the bumper-middle (P03). A larger deformable space (the space between the bumper and bumper fascia) of the bumper-middle location was found comparing the crash-can location. A larger transitional radius of the crash can part can also be noted at the hood leading edge region. The bumper center height was approximately 490 mm.

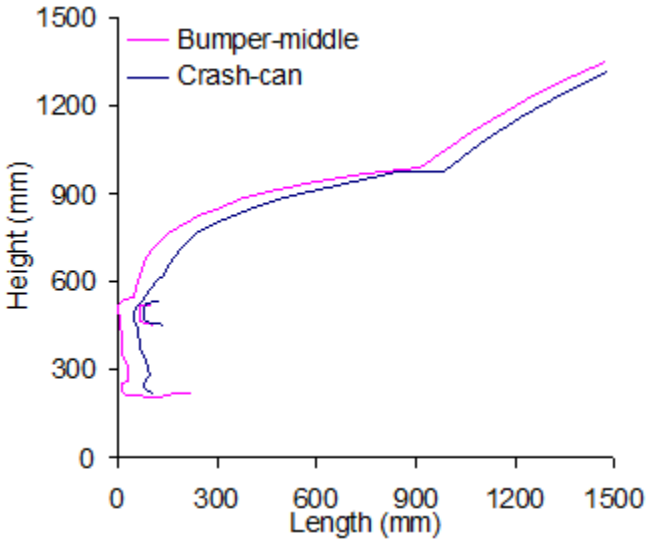

Fig. 3. Front shapes of two locations of the car model.

The relative height of the car bumper to the knee center of the pedestrian is variable due to pedestrian heights, types of cars and impact environments, etc. To study its influence, impact heights were defined to be relevant to pedestrian heights between the 5^{th} and 95^{th} human height percentile (Table 1). These positions were postulated by translating the pedestrian model in the height direction according to the previous anthropometric data of the TNO (1996) study. Considering the previous studies (Arnoux et al., 2006; Matsui, 2005; Mo et al., 2012c), the relative height of the bumper to the knee joint center had essential influences on lower limb injuries. For in-depth investigation of this factor, twelve impact heights on the lower limb were set. The translating displacement is from -60 mm to 50 mm. Each interval is 10 mm.

Table 1 Descriptions of setting different impact heights.

Pedestrian anthropometry	Height (mm)	Scale factors	Knee joint centre (mm)	Translated distances (mm)
5%	1530	0.879	440	-60
50%	1740	1.0000	500	0
95%	1910	1.098	549	+50

In summary, three levels of locations and velocities are defined in the analysis matrix (Table 2). Totally, 108 simulations were implemented to investigate the influence of loading conditions on injury occurrences of the knee ligaments.

Table 2 Simulation matrix of the parametric study.

Factors	Low level	Middle level	High level	Levels
Impact height	-60 mm	0 mm	50 mm	12
Impact location	Crash-can	Mid-point	Bumper-middle	3
Velocity (km/h)	20	30	40	3

RESULTS

Lateral shear displacements were reported in two groups: tibia lateral translation (the positive value of lateral shearing) and tibia medial translation (the negative value of lateral shearing). The positive value of the lateral bending angle corresponds to valgus rotation while the negative value represents varus rotation. Only valgus rotation was found in the current simulations due to the loading condition. These two types of lateral shearing or bending were induced by the relative height of the bumper to the knee joint center.

Influences of impact heights

The initial ligament injury occurrences (namely the first knee injuries during the loading process) are considered to establish the injury threshold. Both MCLs and cruciate ligaments were found as initial knee ligament injuries in the simulations (Fig 4). MCL failures are relevant to high bending values, while cruciate ligaments (especially ACLs) mostly present high positive shearing values. Injury occurrences of the knee ligaments are correlated to impact heights, considering translated displacements of the car model as shown in Fig. 5. The impact height shows significant influence on the initial failure types and the corresponding injury thresholds of bending and shearing. Initial knee injuries of the ACL type were mostly caused by the impacts with the knee joint center lower than the bumper center. Those of the MCL type were mostly related to the impacts above the knee joint center. Only two cases of the PCL type were reported.

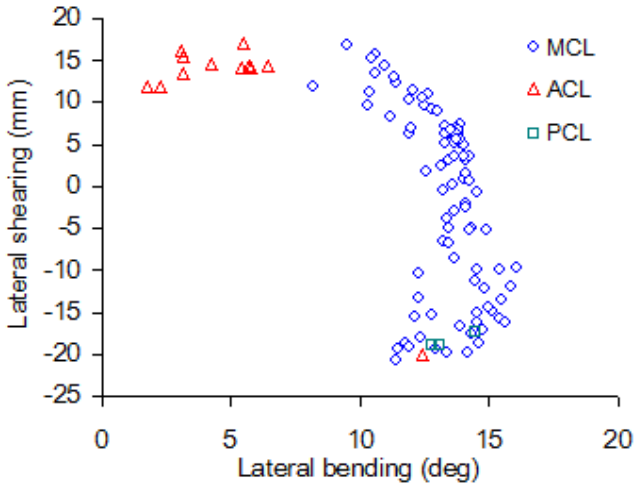

Fig. 4. Injury occurrences of initial knee injuries categorized by ligament types.

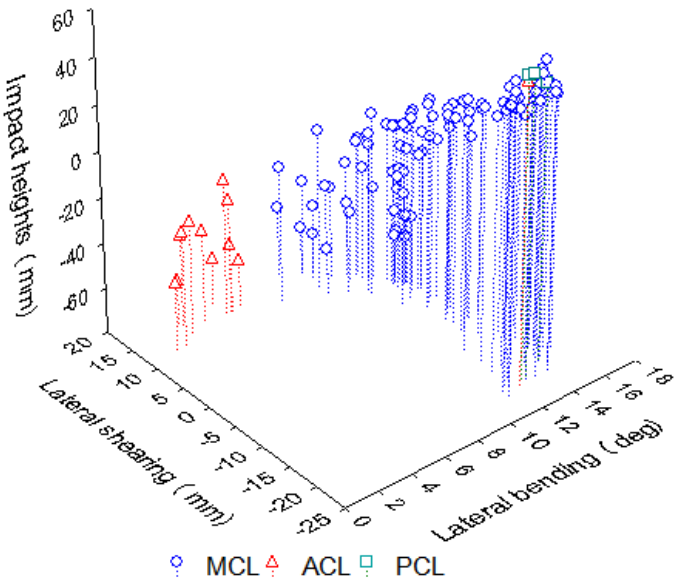

Fig. 5. Influences of impact heights on the injury occurrences.

Influences of impact velocities and locations

Previous experimental test results on the isolated lower limb and knee (Kajzer et al., 1999; Kajzer et al., 1997; Kaneta et al., 2010) revealed that increasing the impact velocity would increase knee injury severity. Especially for bending loading, these test results showed a change from isolated MCL damage to multiple ligament failures when the impact velocity inclined. The current study found that initial injury occurrences of the knee ligaments (including ligament failure types, bending and shearing values at failure) also varied with impact velocities, as shown in Fig. 6. At 20km/h, only the MCL type of initial knee injuries was found. When the impact velocity was increased to 30km/h, initial cruciate ligament failures were noted. Cruciate ligament injuries in the simulations are more frequent at the impact velocity of 40 km/h. In addition, the contour of bending and shearing values at ligament failure time of 20 km/h impacts present essential differences with the impacts of other velocities.

Fig. 6. Influences of impact velocities on the injury occurrences.

Matsui et al. (2011) implemented the experimental tests of the lower legform impactor on the center and side position of different types of cars. The test results revealed that the side position of cars (in front of car longitudinal beams) is more aggressive to the knee joint than the bumper center position. The current simulations indicate that the highest frequency of initial cruciate ligament injuries appear in the P01 location (in front of the crash can and longitudinal beam), as shown in Fig. 7. Eleven of 15 cases of initial cruciate ligament injuries were due to impacts on the P01 location. In addition, the contour shaped by bending and shearing values at ligament failure time does not show significant difference regarding these impact locations.

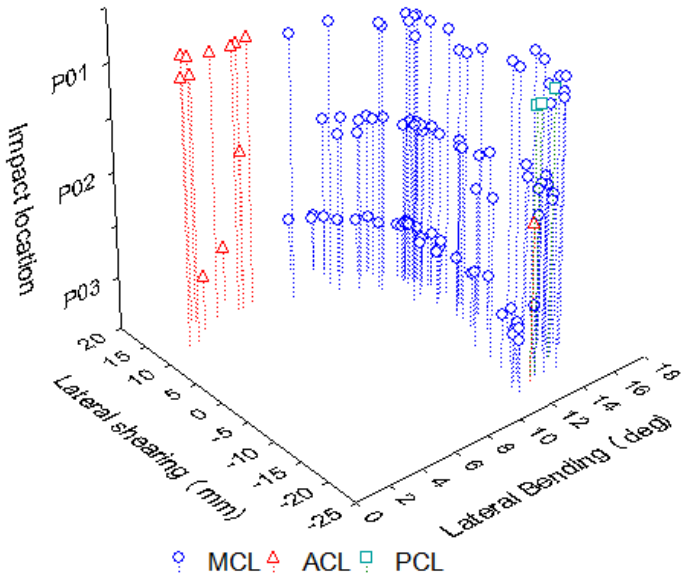

Fig. 7. Influences of impact locations on the injury occurrences.

DISCUSSION

The knee presents multiple injuries related to complex joint kinematics in the car-pedestrian impact environment. Although general injury mechanisms of the knee joint can be determined in full-scale pedestrian experiments, the quantitative correlation of joint kinematics to knee injuries was not investigated fully due to the limited tools for calculating joint kinematics values. To understand this correlation, the current study employed the method of finite element simulation including a biofidelic lower limb model with the entire human body inertia and a new generation car model. Thus the corresponding joint kinematics related to knee injuries can be acquired accurately by analyzing the simulation results. In addition, the previous full-scale vehicle-pedestrian experiments with cadavers revealed that many factors influence knee injury occurrences, such as impact velocities, impact heights on the lower limb and the front-end shape of the vehicle (Kerrigan et al., 2008; Masson et al., 2007). Therefore, we employed a parametric study to evaluate the sensitivity of these factors by simulating pedestrian loading conditions in the collision with the car.

As initial cruciate ligament failures recorded in the impact simulation of the crash can position were more frequent than the other two positions (Fig. 7), it could reveal that this position is more aggressive to pedestrian knees. According to the front-end shape of different

locations presented in Fig. 3, the smaller deformable space and larger transitional radius around the hood leading edge could be the incidence to this phenomenon. A smaller deformable space indicates higher stiffness. A larger transitional radius could induce a large lateral bending angle of pedestrian lower limbs more easily when the impact occurs between the pedestrian and the car. The influence of impact heights on the injury tolerances of both long bones and knee joints have been largely discussed in the previous studies (Arnoux et al., 2006; Matsui, 2005; Mo et al., 2012b; Mo et al., 2012c). Substantial effects of impact heights were also noted in the current study. Considering the overall results, MCL injuries were principally due to combined bending and shearing effects, while initial ACL injuries were related to large shear displacements induced by high impact positions. These injury mechanisms are consistent with previous isolated lower limb experiments (Kajzer et al., 1999; Kajzer et al., 1997). These experiments revealed that the shearing test represents a large proportion of ACL failures, and the bending test corresponds to a large proportion of MCL injuries. Furthermore, regarding the influence of impact heights (Fig. 5), the current results report that increasing the impact height on the lower limb would increase the risk of primary cruciate ligament injuries. Considering the impact height influence, this finding is relevant to the previous full-scale pedestrian experiments of Kerrigan et al. (2008), which reported that 11 of 12 cruciate ligaments in the SUV (sport utility vehicle) tests versus only 2 of 12 in the sedan tests suffered complete ruptures. The authors indicated that the higher bumper of the SUVs and other additional structural characteristics could be responsible for this potential difference.

Under the lateral car-pedestrian impact, knee injuries have been principally attributed to lateral bending and shearing mechanisms induced by vehicle bumpers (Yang, 2005). In the current simulations, the knee impact responses of lateral bending and shearing were also found to be the dominant factors associated with the knee injuries. Lateral bending consisted of tibia varus rotation and tibia valgus rotation. Lateral shearing included tibia medial translation and tibia lateral translation. Other joint motions with potential influences were also noted, such as tibia internal/external rotation and tibia proximal/distal translation. These knee impact responses were mainly responsible for the substantial variance between tibia medial translation values and tibia lateral translation values when initial injuries occurred at the same bending level (Fig. 4). Two cases of the typical knee impact responses in the parametric study are shown in Fig. 8. Positive values are from tibia internal rotation, tibia distal translation and tibia lateral translation, while negative values represent tibia external rotation, tibia proximal translation and tibia medial translation (Fig. 8). The tibia lateral translation usually appeared with the tibia internal rotation and a low tibia distal translation value. The tibia medial translation occurred with the tibia proximal translation and a large tibia internal rotation value.

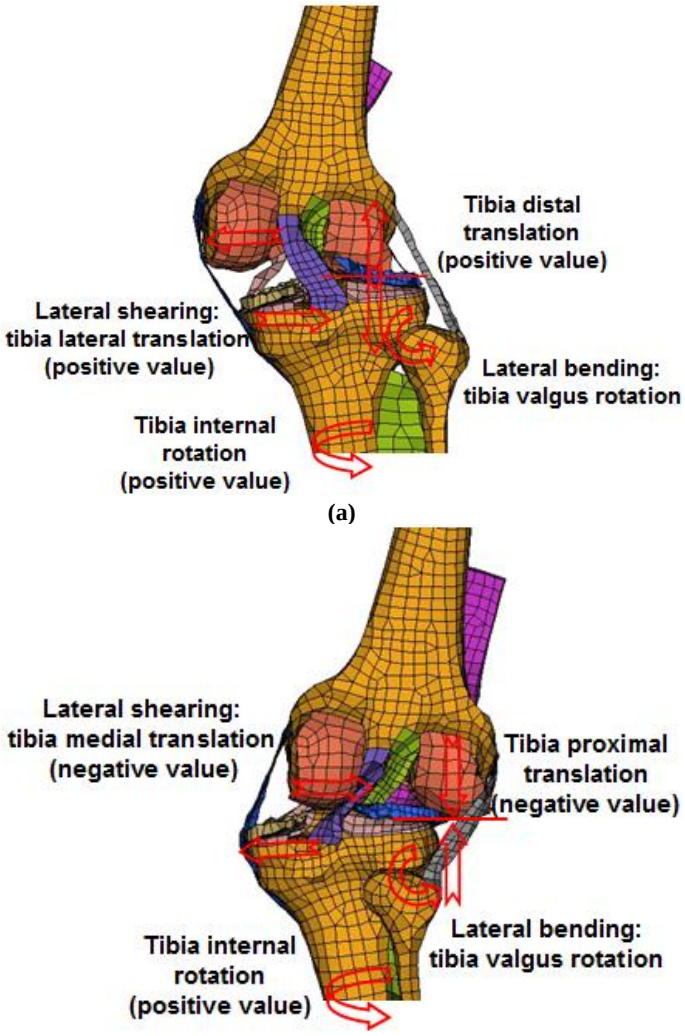

Fig. 8. Typical knee joint kinematics: (a) positive lateral shearing and (b) negative lateral shearing.

The influences of tibia internal/external rotation and tibia distal/proximal translation on the combined bending and shearing thresholds for initial ligament injuries are shown in Fig. 9 and Fig. 10, respectively. It appears that the failure points with large tibia internal rotation value and tibia proximal translation value would possess high bending and shearing values comparing the points without these joint kinematic responses. From a medical point of view, tibia internal/external rotation (or torsion) could protect knee ligaments injuries as indicated by Masson et al. (2005). Influences of tibia distal/proximal translation on the combination of bending and shearing are evident. From knee joint kinematics shown in Fig. 8, tibia distal translation extends ligaments of the knee joint, while tibia medial translation compresses the joint and reduces the elongation of knee ligaments. Hence, the cases with tibia medial translation (negative shearing values) exhibited larger absolute bending and shearing values compared to the ones with tibia lateral translation (positive shearing values) due to the influences of tibia proximal translation and tibia internal rotation (Fig.4).

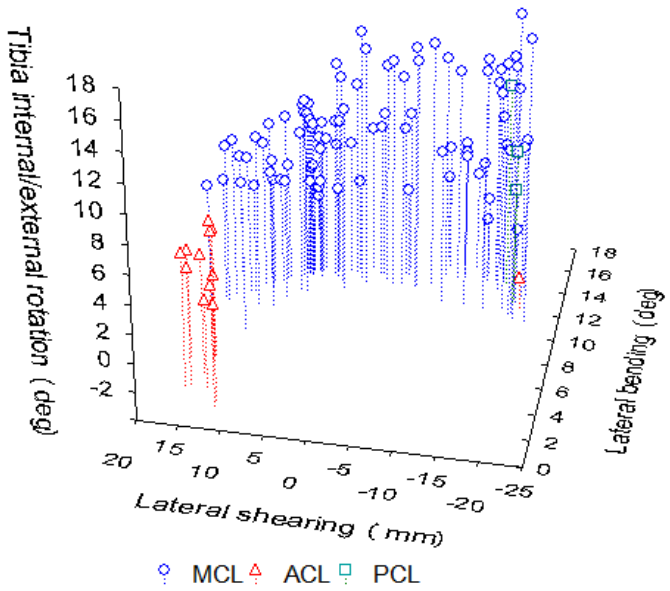

Fig. 9. Influences of tibia internal/external rotation on the combined bending and shearing thresholds.

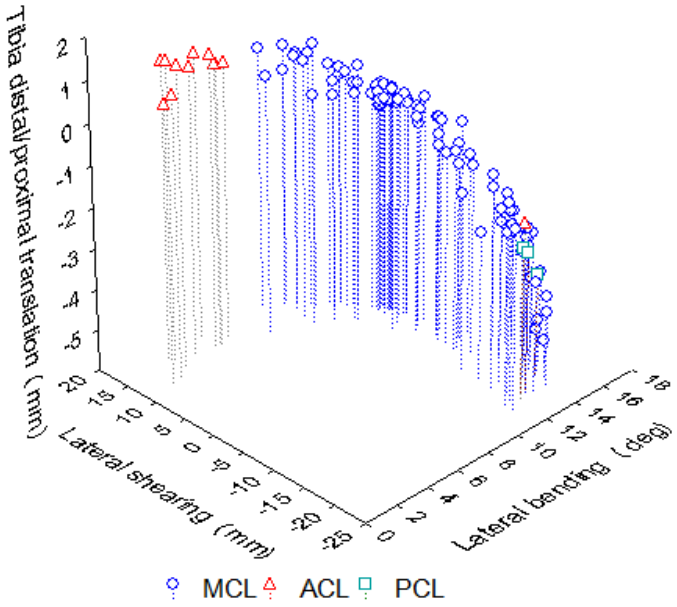

Fig. 10. Influences of tibia distal/proximal translation on the combined bending and shearing thresholds.

In addition, high combined bending and shearing values under tibia medial translation could also be related to the method limitation of the model for predicting ligament injury. The global strain thresholds (24% for cruciate ligaments and 28% for collateral ligaments) of the ligaments were used to predict failure risk of the knee ligaments in the current study. Non-homogenous local strain distributions of ligaments can be found in the FE simulations, especially for cruciate ligaments that exhibited a complicated interaction with the bone articulation. The diverse modes of local strain distribution were determined by the knee impact responses caused by different loading conditions, which were in particular related to the relative height of the bumper to the knee center. Regarding the typical knee impact responses in Fig. 8.b, the interaction of the PCL, femoral medial condyles and tibial eminences would lead to substantial local deformation of the PCL around its tibial attachment. This indicates the PCL could rupture before reaching the global strain threshold due to the evident concentration of the local deformation. However, only two cases of initial PCL failures under tibia medial translation were found in the simulations. According to the

previous experiments of the car-pedestrian impact (Kerrigan et al., 2008; Masson et al., 2007), although the PCL was not as frequently injured as the MCL and ACL, failures were not so rare. Additionally, the global strian of the entire ligament is also influenced by the selected locations of the measuring springs. If the ligament is directly streched without large deformation in other directions, this influence is non-significant. If the ligament is largely bended, the deformation of interior elements could be significantly different with exterior ones. In our simulations, we noted that the interaction between ligaments and bone structures could lead the ligaments bend slightly around femoral doncyles. In the model, we seleted the middle line of the entire ligament to define these spring sensors that would limit the influence of this bending deformation. However, the method used for predicting ligament failures in this paper could be still improved in future works. Hence, although the global thresholds were based on the experimental results and validated through the complex loading conditions, its application for injury prediction still could not cover all the loading environments in the car-pedestrian impact, in particular in the case of tibia medial translation. On the other hand, we also worked on ligament failure implementation with the ultimate strain applied in the shell and solid elements (Mo et al., 2012a). However, the common FE method simulates structural failures by deleting elements in the simulation. So the failure modeling is very sensitive to the element size. To a global lower limb model for safety research, the mesh for representing ligaments is still not refined enough due to the consideration of the time step and model stability. If we directly implement element failure in the ligament, it could overestimate ligament failures by the crack size, which is determined by the element size. That means a physical small laxity could be reflected as a total rupture in the model due to the relatively large element size. Using the global strain of the entire ligament to evaluate the ligament failure would avoid this situation. In the future, the model and its failure modeling method should be continually developed. One solution could be the extended finite element method (XFEM), which has been recently developed to be available in commercial FE softwares, and presented its advantage in modeling actual crack initiation and growth (Elkins et al., 2013). The corresponding experimental tests should be also implemented to determine the lateral shear threshold of the knee joint.

In summary, as we noted in these simulations reflecting realistic car-pedestrian impact environments, the injury occurrence of the knee ligaments is principally determined by a varying combination of lateral bending and shearing, which is also influenced by tibia internal/external rotation and tibia proximal/distal translation. In comparison with the cases of tibia lateral translation, tibia medial translation corresponded to higher combined bending and shearing thresholds due to the influence of tibia internal/external rotation and tibia proximal/distal translation. In addition, this phenomenon may be also related to the modeling method for predicting the ligament injury, as discussed above.

Because of these reasons, cases from the parametric study with tibia lateral translation were considered in developing the injury thresholds of the knee ligaments based on the dominant injury mechanisms. Regarding different injury occurrences as shown in Fig. 4, the initial knee ligament injuries could be divided into two categories: ACL failure that is dominated by lateral shearing level and MCL failure that is determined by the combined effect of lateral bending and shearing. The development of the injury threshold is shown in Figure 11. The injury threshold of the ACL was defined as the mean value of lateral shear displacement corresponding to initial ACL failure occurrences. A quadratic regression curve correlating lateral shearing to lateral bending was developed for initial MCL injury occurrences. For the

robustness and accuracy of the regression, both initial and ensuing injury occurrences of the MCL are considered in the development, as shown in Figure 11. The ensuing MCL failures after cruciate ligament injuries are exhibited in the rectangular frame. Finally, a typical injury threshold was determined for the impacts of 40 km/h as a closed contour composed of the shearing threshold and one part of the quadratic injury function (Figure 11 and Figure 12).

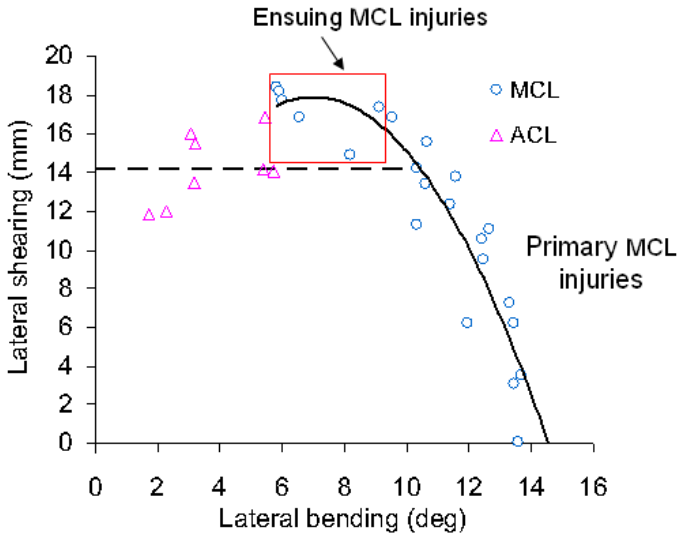

Fig. 11. Development of the injury threshold of the knee joint under 40km/h.

The same method was used to develop the injury threshold for the impacts of 30km/h. The injury occurrences under 20km/h were mostly related to tibia medial translation with the isolated MCL injury type. Thus, its injury threshold was not proposed. In the previous study of Mo et al. (2012c), an injury criterion was defined based on the isolated lower limb tests at 20km/h. As the car-front end shape was not involved in the tests, the knee response was not as complicated as noted by the car-pedestrian impact simulation in the current study. Only tibia lateral translation was found due to the loading condition. The significant influences of other knee impact responses were also not well noted as in the current study.

All the injury functions described above are shown in Fig. 12 and Table 3. These functions are in general agreement regardless of loading types (the isolated lower limb impact or the car-pedestrian impact) and velocities. For 20 km/h, 30km/h and 40 km/h, the corresponding shear levels are similar with an average value of 14.2mm (Standard Deviation= 0.5). We developed these thresholds by considering the dominant injury mechanisms of the knee ligaments – lateral bending and shearing. The small variation could be explained by coupled effects of the complex kinematics as well as testing conditions. As we previously described, in Mo et al. (2012c) the MCL part of the 20 km/h injury threshold is close to the coupling injury criteria proposed by Bose et al. (2008) based on experimental results. The shear threshold is also close to the previously defined shear levels from experimental tests that are listed in the introduction (Bhalla et al., 2003; Kajzer et al., 1999; Kajzer et al., 1997; Kerrigan et al., 2003; Ramet et al., 1995). In the current study, this agreement further demonstrated that the previous injury criteria proposed by Mo et al. (2012c) is available to evaluate knee ligament injuries in many cases of the car-pedestrian impact conditions. In summary, a closed contour could be defined as the injury threshold for the pedestrian knee joint: a unique lateral shearing level around 14mm when lateral bending was smaller than approximately 10 degrees, coupled with a quadratic function with an end at lateral bending angle of around 16

degrees (Fig. 12 and Table 3).

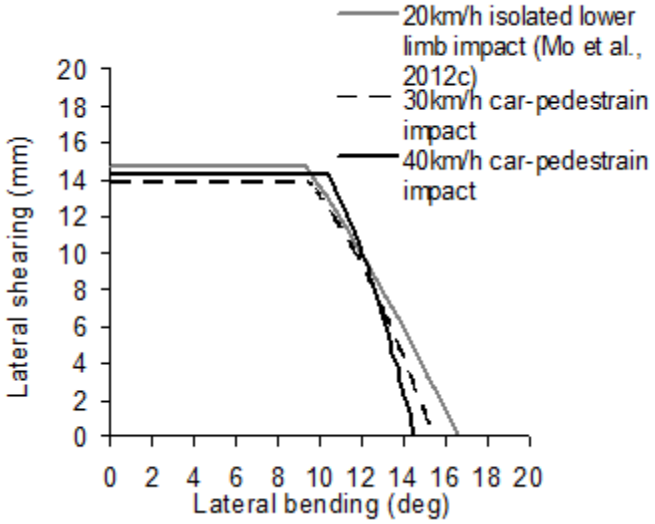

Fig. 12. Knee injury thresholds at different impact velocities.

Table 3 Summary of the knee injury functions at different velocities ($D_{shearing}$ represents lateral shear displacement of the knee and $B_{bending}$ is lateral bending angle of the knee).

	Knee injury thresholds
20km/h isolated lower limb impact (Mo et al., 2012c)	$D_{shearing} = 14.7mm, (0^\circ \le B_{bending} \le 9.3^\circ)$ $D_{shearing} = -0.054B_{bending}^{\ 2} - 0.62B_{bending} + 25.05$ $(B_{bending} \ge 9.3^\circ,\ R^2 = 0.99)$
30km/h car-pedestrian impact	$D_{shearing} = 13.8mm, (0^\circ \le B_{bending} \le 9.5^\circ)$ $D_{shearing} = -0.16B_{bending}^{\ 2} + 1.65B_{bending} + 12.62$ $(B_{bending} \ge 9.5^\circ,\ R^2 = 0.67)$
40km/h car-pedestrian impact	$D_{shearing} = 14.2mm, (0^\circ \le B_{bending} \le 10.4^\circ)$ $D_{shearing} = -0.31B_{bending}^{\ 2} + 4.41B_{bending} + 2.48$ $(B_{bending} \ge 10.4^\circ,\ R^2 = 0.86)$

In addition, other passenger vehicles with various front-end shape designs should be used to evaluate the efficiency of the presented injury threshold and promote its robustness development, such as large family cars, SUVs, MPVs. For the impact height, the current study aims to investigate the relative height of the pedestrian knee center to the car bumper. We introduce the pedestrian height to cover the possibility of relative impact heights. If we scale this combined pedestrian model, many factors could not be proper considering the geometry and element. Regarding the principal objective, we translate the car model to approach these relative impact heights and to keep the originality and validity of the pedestrian model. In the future, the influence of pedestrian heights could be investigated by scaling the model geometry.

There are still several aspects that could be investigated to improve the robustness of the

current thresholds. First, due to the specific front-end shape and the definition of the current parametric study, the varus rotation of lateral bending was not found in the simulations. This could also be the reason that initial LCL failures were not noted in the current study. LCL failures usually existed in the counter knee joint without first contact on the vehicle, as revealed by the experimental results of the full-scale pedestrian tests (Kerrigan et al., 2008; Masson et al., 2007). The relative height of the vehicle bumper to the pedestrian knee joint center is responsible for this phenomenon. In this case, initial LCL injuries could be really rare in car-pedestrian accidents. Nevertheless, it would still be interesting to improve the current injury thresholds with the consideration of this injury type. Second, only the rupture of knee ligaments was the focus of the current study. In the future, other injury types of the knee joint (including fractures of the femoral and tibial epiphyses, menisci and cartilage damage) should be also addressed to finalize the defined injury thresholds of the entire knee joint. Regarding previous experimental works (Bose et al., 2008; Kajzer et al., 1999; Kajzer et al., 1997; Kerrigan et al., 2003), an injury threshold reproducing a combination of shear force and bending moment could be developed to evaluate these knee injuries considering the ultimate stress or strain of corresponding structures. Third, as investigated in many previous studies (Kajzer et al., 1999; Kajzer et al., 1997; Kerrigan et al., 2003), the dominant injury mechanisms of the knee ligaments are lateral bending and shearing. Thus, we considered the coupling of these mechanisms to develop the injury thresholds. As we previously discussed, other joint kinematics (tibia distal/proximal translation and tibia internal/external rotation) would also influence the combination of bending and shearing. In particular, the effects of tibia distal/proximal translation were significant. Due to simulation data and DOE design in the present work, we considered that it was not possible to implement all these effects to establish injury thresholds. The robustness of the current thresholds could be improved by considering all these influences. In addition, the effect of different age groups is not included in the definition of model materials. The model can be improved in this aspect to investigate the influence of aging on injury occurrences of the knee ligaments.

CONCLUSION

A parametric study of car-pedestrian impact conditions was implemented through finite element simulations. The influences of three impact factors (impact heights, locations and velocities) on injury occurrences of the knee ligaments were discussed. The relative impact height of the knee center to the bumper beam center presented significant influences on initial ligament injury types. It also induces an evidently varying combination of bending and shearing levels at failure occurrences of the ligaments.

Regarding initial ligament injuries, the injury thresholds of the knee ligaments were established through dominant injury mechanisms – lateral bending and shearing. Overall simulation results also show the influences of other knee responses (tibia distal/proximal translation and tibia internal/external rotation) on the combination of lateral bending and shearing. In addition, the currently developed thresholds by simulating car-pedestrian impact conditions are well correlated with previously proposed criteria. In this case, it demonstrated that the previous criteria could be used to evaluate knee ligament injuries of pedestrians in collisions with cars. More vehicle models are needed to assess the current injury thresholds through FE simulations or experimental tests.

References

Arnoux, P.J., 2000. Modélisation des ligaments des membres porteurs. Ph.D. thesis. Université de la Méditerranée, Marseille, Paper.

Arnoux, P.J., Cavallero, C., Chabrand, P., Brunet, C., 2002. Knee ligament failure under dynamic loadings. International Journal of Crashworthiness 7, 255-268.

Arnoux, P.J., Cesari, D., Behr, M., Thollon, L., Brunet, C., 2005. Pedestrian lower limb injury criteria evaluation: a finite element approach. Traffic Injury Prevention 6, 288-297.

Arnoux, P.J., Thollon, L., Behr, M., Brunet, C., Cesari, D., 2006. Knee joint injury mechanisms and injury criteria in full scale tests according to impact position, 2006 International Research Council on Biomechanics of Injury (IRCOBI) Conference, Madrid, Spain, pp. 319-322.

Banglmaier, R.F., Dvoracek-Driskna, D., Oniang'o, T.E., Haut, R.C., 1999. Axial compressive load response of the 90 degrees flexed human tibiofemoral joint, 43rd Stapp Car Crash Conference, San Diego, CA, pp. 127-138.

Beillas, P., Begeman, P.C., Yang, K.H., King, A.I., Arnoux, P.J., Kang, H.S., Kayvantash, K., Brunet, C., Cavallero, C., Prasad, P., 2001. Lower Limb: Advanced FE Model and New Experimental Data. Stapp Car Crash Journal 45, 469-494.

Beillas, P.D., 1999. Modélisation des membres inférieurs en situation de choc automobile. Ph.D. thesis. École Nationale Supérieure d'Arts et Métiers, Paris, France.

Bhalla, K., Bose, D., Madeley, N.J., Kerrigan, J., Crandall, J., 2003. Evaluation of the response of mechanical pedestrian knee joint impactors in bending and shear loading, 18th International Technical Conference on the Enhanced Safety of Vehicles (ESV), Nagoya, Japan, Paper No. 429.

Bose, D., Arnoux, P.J., Cardot, J., Brunet, C., 2007. Evaluation of knee injury threshold in pedestrian-car crash loading using numerical approach. International Journal of Crashworthiness 12, 381-399.

Bose, D., Bhalla, K., Rooij, L., Millington, S., Studley, A., Crandall, J., 2004. Response of the knee joint to the pedestrian impact loading environment, SAE 2004 World Congress & Exhibition, Detroit, Michigan, USA, Paper No. 2004-01-1608.

Bose, D., Bhalla, K.S., Untaroiu, C.D., Ivarsson, B.J., Crandall, J.R., Hurwitz, S., 2008. Injury tolerance and moment response of the knee joint to combined valgus bending and shear loading. Journal of Biomechanical Engineering-Transactions of the Asme 130, 031008-1-8.

Cater, E.L., Neal-Sturgess, C.E., Hardy, R.N., 2008. APROSYS in-depth database of serious pedestrian and cyclist impacts with vehicles. International Journal of Crashworthiness 13, 629-642.

Commission of the European Communities, 2003. Proposal for a directive of the euopean parliament and of the council relating to the protection of pedestrians and other vulnerable road users in the event of a collision with a motor vehicle and amending directive 70/156/eec, Brussels.

Elkins J, Pedersen D, Callaghan J, Brown T. Do Obesity and/or Stripe Wear Increase Ceramic Liner Fracture Risk? An XFEM Analysis. Clin Orthop Relat Res. 2013;471(2):527-536.

European Experimental Vehicles Committee: Working Group 10 on Pedestrian Proctection, 1994. Proposals for methods to evaluate pedestrian protection for passenger cars: Final report.

European Experimental Vehicles Committee: Working Group 17 on Pedestrian Proctection, 1998. Improved test methods to evaluate pedestrian protection afforded by passenger cars.

Grood, E.S., Suntay, W.J., 1983. A joint coordinate system for the clinical description of 3-dimensional motions- application to the knee. Journal of Biomechanical Engineering-Transactions of the Asme 105, 136-144.

Haut, R.C., Atkinson, P.J., 1995. Insult to the human cadaver patellofemoral joint: effect of age on fracture tolerence and occult injury, 39th Stapp Car Crash Conference, Tempe, AZ, Paper No. 952729.
Hayashi, S., Choi, H.Y., Levine, R.S., Yang, K.H., King, A.I., 1996. Experimental and analytical study of knee fracture mechanisms in a frontal knee impact, 40th Stapp Car Crash Conference, Albuquerque, New Mexico, Paper No. 952729.
International Harmonized Research Activities (IHRA), 2001. Pedestrian safety working group 2001 report.
Jundt, G., 2007. Modéles d'endommagement et de rupture des matériaux biologiques. Ph.D. thesis. Université de la Méditerranée, Marseille.
Kajzer, J., Cavallero, C., Bonnoit, J., Morjane, A., Ghanouchi.S., 1990. Response of the knee joint in lateral impact: Effect of shearing loads, 1990 International Research Council on Biomechanics of Injury (IRCOBI) Conference, Bron-Lyon, France, pp. 293-304.
Kajzer, J., Cavallero, C., Bonnoit, J., Morjane, A., Ghanouchi.S., 1993. Response of the knee joint in lateral impact: Effect of bending loads., 1993 International Research Council on Biomechanics of Injury (IRCOBI) Conference, Eindhoven,The Netherlands pp. 105-116.
Kajzer, J., Matsui, Y., Ishikawa, H., Schroeder, G., 1999. Shearing and bending effects at the knee joint at low speed lateral loading, SAE 1999 World Congress & Exhibition, Detroit, Michigan, USA, Paper No. 1999-01-0712.
Kajzer, J., Schroeder, G., Ishikawa, H., Matsui, Y., 1997. Shearing and bending effects at the knee joint at high speed lateral loading, SAE 1997 World Congress & Exhibition, Detroit, Michigan, USA, Paper No. 973326.
Kaneta, Y., Sasahara, N., Kusama, I., Suzuki, D., Ohkawa, H., Hara, T., 2010. Injury tolerance of knee joint subjectd to dynamic three-point bending. Jouranl of Biomechanical Science and Engineering 5, 94-103.
Kerrigan, J., Rudd, R., Subit, D., Untaroiu, C., Crandall, J., R., R., 2008. Pedestrian lower extremity response and injury: A small sedan versus a large sport utility vehicle, SAE 2008 World Congress & Exhibition, Detroit, Michigan, USA, Paper No. 2008-01-1245.
Kerrigan, J.R., Bhalla, K.S., Madeley, N.J., Funk, J.R., Bose, D., Crandall, J.R., 2003. Experiments for establishing pedestrian-impact lower limb injury criteria, SAE 2003 World Congress & Exhibition, Detroit, Michigan, USA, Paper No. 2003-01-0895.
Masson, C., Arnoux, P.J., Brunet, C., Cesari, D., 2005. Pedestrian injury mechanisms & criteria: A coupled experimental and finite element approach, 19th International Technical Conference on the Enhanced Safety of Vehicles Conference (ESV), Lyon, France, Paper No. 05-0335.
Masson, C., Serre, T., Cesari, D., 2007. Pedestrian-vehicle accident: analysis of 4 full scale tests with PMHS, 20th International Technical Conference on the Enhanced Safety of Vehicles Conference (ESV), Lyon, France, Paper No. 07-0428.
Matsui, Y., 2005. Effects of vehicle bumper height and impact velocity on type of lower extremity injury in vehicle–pedestrian accidents. Accident Analysis & Prevention 37, 633-640.
Matsui, Y., Hitosugi, M., Mizuno, K., 2011. Severity of vehicle bumper location in vehicle-to-pedestrian impact accidents. Forensic Science International 212, 205-209.
Mo, F., Arnoux, P.J., Cesari, D., Masson, C., 2012a. The failure modelling of knee ligaments in the finite element model. International Journal of Crashworthiness, 2012. 17(6): p. 630-636.
Mo, F., Arnoux, P.J., Jure, J.J., Masson, C., 2012b. Injury tolerance of tibia for the car–pedestrian impact. Accident Analysis & Prevention 46, 18-25.

Mo, F., Masson, C., Cesari, D., Arnoux, P.J., 2012c. Coupling lateral bending and shearing mechanisms to define knee injury criteria for pedestrian safety. Traffic Injury Prevention, 2012. DOI:10.1080/15389588.2012.721146.
Nyquist, G., Cheng, R., EI-Bohy, A., King, A., 1985. Tibia bending: Strengh and response, SAE 1985 World Congress & Exhibition, Detroit, Michigan, USA, pp. 99-112, Paper No. 851728.
Obervatoire National Interministériel de la Sécurité Routière, 2011. La sécurité routière en france: Bilan de l'année 2010, Paper.
Peten, M., Scrurfield, R., Sleet, D., Mohan, D., Hyder, A.A., Jarawan, E., Mathers, C., 2004. World report on road traffic injury prevention. World Health Organization, Geneva,Switzerland.
Ramet, M., Bouquet, R., Bermond, F., Caire, Y., 1995. Shearing and bending effects at the knee joint tests in quasi-static lateral load, 1995 International Research Council on Biomechanics of Injury (IRCOBI) Conference, Brunnen, Switzerland, pp. 93-105.
Teresinski, G., Madro, R., 2001. Knee joint injuries as a reconstructive factors in car-to-pedestrian accidents. Forensic Science International 124, 74-82.
TNO., 1996. MADYMO User's Manual 3D, Version 5.2. Road Vehicles Research Institute, Delft, The Netherlands.
Viano, D.C., Culver, C.C., Haut, R.C., Melvin, J.W., Bender, M., Culver, R.H., Levine, R.S., 1978. Bolster impacts to the knee and tibia of human cadavers and an anthropomorphic dummy, 22nd Stapp Car Crash Conference, New York, p. 401, Paper No. 780896.
Weiss, J.A., Gardiner, J.C., 2001. Computational modeling of ligament mechanics. Critical Reviews in Biomedical Engineering 29, 303-371.
Yang, J.K., 2005. Review of injury biomechanics in car-pedestrian collisions. International Journal of Vehicle Safety 1, 100-117.

Chapitre 2 :

Incidence du design de la face avant du véhicule sur la vulnérabilité du membre pelvien

Ce premier chapitre est présenté sous la forme d'un papier intitulé « Evaluation of injury thresholds of lower extremities by FE simulations of full-scale vehicle-pedestrian impacts » par Fuhao Mo, Massimiliano Avalle, Alessandro Scattina, Elena Semino, Catherine Masson Pierre Jean Arnoux en cours de révision à l'international Journal of Crashworthiness.

INTRODUCTION

During the past three decades, injury biomechanics in vehicle-pedestrian collisions has been extensively studied. By the analysis of accidental data, passenger vehicles have been proved to be responsible for most pedestrian injuries (Mallory and Stammen, 2006,Gavrila, et al., 2003). Pedestrian lower extremities are the most frequently injured body region (IHRA 2001,Cater, et al., 2008) and their injuries analysis are continuously concerned by researchers using research methods of both experimental tests and finite element simulations (Arnoux, et al., 2005,Yasuki, 2007,Mo, et al., 2012,Masson, et al., 2007,Kerrigan, et al., 2008).

The European Enhanced Vehicle-safety Committee (EEVC WG17, 1998,EEVC WG10, 1994) proposed a series of subsystem impactor tests to evaluate the aggressiveness of passenger vehicles to pedestrians. Based on these proposals, European commission directive 2003/102/EC enacted a lower leg impactor test procedure to improve passenger vehicles design and mitigate pedestrian lower extremity injuries. This test procedure used a mechanical legform developed by the Transport Research Laboratory (TRL) to represent a lower extremity of the human body. Many studies have addressed the problems of both the legform and injury criteria used by this test procedure (Yasuki, 2007,Mo, Arnoux, Jure,Masson, 2012,Yasuki, 2007,Mo, et al., 2012,Martinez, et al., 2008). After this, the Japan Automobile Research Institute (JARI) and the Japan Automobile Manufacturer Association (JAMA) developed a Flexible Pedestrian legform Impactor (Flex-PLI). It has flexible tibia and femur components mainly made from a high strength plastic with a fiber reinforced bone on the inside. The knee component is also flexible with four major ligaments made of springs and stainless steel wires. The elongation of ligaments was measured to evaluate potential knee injuries in the legform. Global technical regulation No.9 of Economic Commission for Europe (ECE) presented the application of Flex-PLI on pedestrian protection (Committee, 2010). To guide improvement of passenger vehicle design for pedestrian protection, all these legform tests should be available to reflect real-world impact environments. Thus, the full-scale vehicle-pedestrian impact test is the basis of developing and improving these regulation tests. Owing to the development of computer modeling, full-scale vehicle-pedestrian impacts can be currently achieved by numerial simulations with low cost comparing experimental methods.

The objective of the present study is to investigate the influence of various passenger vehicle front end structures on lower extremity injuries by realistic vehicle-pedestrian impact simulations. A biofidelic lower extremity model and 4 passenger vehicle models of different

types were included in finite element simulations. Tibia bending moments and knee ligament strains were measured as indexes to evaluate the injury risk of tibia fractures and ligament ruptures. From the analysis of lower extremity kinematics and these indexes, the influences of vehicle front end design on tibia and knee ligaments injuries were discussed to promote the improvement of passenger vehicle front end design for pedestrian protection.

I. MATERIAL AND METHODS

Vehicle-pedestrian impact models

To investigate the influence of various vehicle front-end designs on pedestrian lower extremity injuries, vehicle-pedestrian impacts were replicated for 4 deformable vehicle models including Super Mini (SM), Small Family Car (SFC), Executive Car (EC), and Multi Purpose Vehicle (MPV). These vehicle FE models included detailed structural and material properties, and were successfully used to simulate vehicle-pedestrian impacts (Mo, Arnoux, Jure,Masson, 2012), especially in APROSYS project. All impacts are in the lateral direction with a vehicle traveling velocity of 40 km/h. As shown in Fig. 1, the vehicle models show various bumper beam sections, front end shapes as well as the deformable space between the bumper fascia and beam. The MPV presents a significantly different front end shape and highest bumper beam (515±75 mm), followed by the SM (490±35 mm), the SFC (480±60 mm), finally the EC (460±70 mm). Apart from the SM, other vehicle models included foam absorbers between the bumper fascia and bumper beam. All finite element simulations were implemented using Radioss codes.

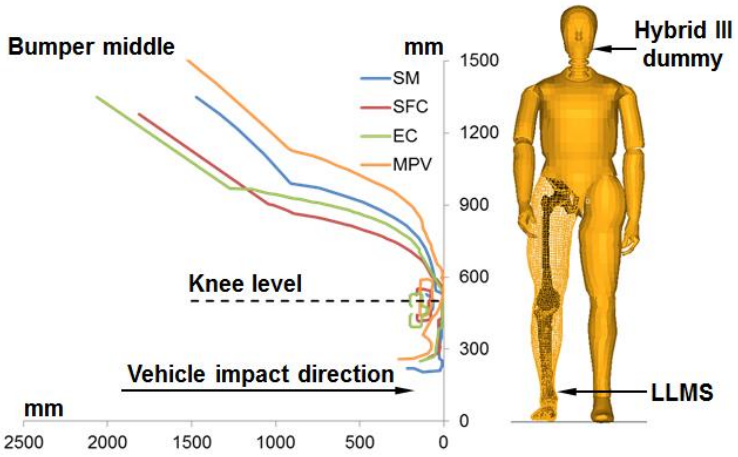

Fig. 1 Passenger vehicle-pedestrian impact models

The pedestrian model is established by combining a 50% Hybrid-III dummy model and a biofidelic lower extremity model at the hip joint. The knee joint center height of the pedestrian is approximately 500 mm. The application of the Hybrid-III dummy model is to consider the entire human body mass and inertial effects during the simulation. The lower extremity model is “Lower limb model for safety” (LLMS) model. It is based on a detailed description of a lower extremity anatomy derived from MRI scans collected on a subject close to a 50th percentile male. The scanning step was 1 mm in the joint region and ranged from 5 mm to 10 mm in other regions. The model was meshed with shells, bricks, or springs depending on anatomical structures. The contacts between bones, ligaments and cartilages were modelled with multipurpose contacts. Most material properties of the model were derived from the literature. Details to support modelling choices were presented in previous

studies (Arnoux, Cesari, Behr, Thollon,Brunet, 2005,Mo, Masson, Cesari,Arnoux, 2012,Beillas, et al., 2001). Compact and spongy bone are modeled by an elastoplastic material, representing knee and patellar ligaments by a generalized viscoelastic material and cartilage and meniscus properties using an elastic material.. This model has been validated at three levels: isolated tissues, sub segments and the entire lower extremity, such as ligament properties under tensile loading, the knee joint response under valgus bending, tibia properties under quasi-static and dynamic bending, and the evaluation of kinematic response of the entire lower extremity (Beillas et al., 2001, Arnoux et al., 2005, Bose et al., 2007, Mo et al., 2012c).

Measurements in the simulation

Tibia bending moments and knee ligament strains were recorded to indicate the injury risk of the corresponding structures. Tibia bending moments of different regions were measured from sections defined at approximately each layer of tibial elements along the tibial axial direction. Knee ligament strains were measured from the deformation of springs along ligament fiber axes (Fig. 2). In addition, lower extremity kinematics were also recorded by several nodes along tibial and femoral axes, in order to determine the influence of vehicle front end shape and stiffness on injury occurrences of the tibia and knee ligaments. In particular, lateral bending and shearing are extracted by the relative angle of vectors and relative displacement of points in the lateral direction, respectively (Fig. 2).

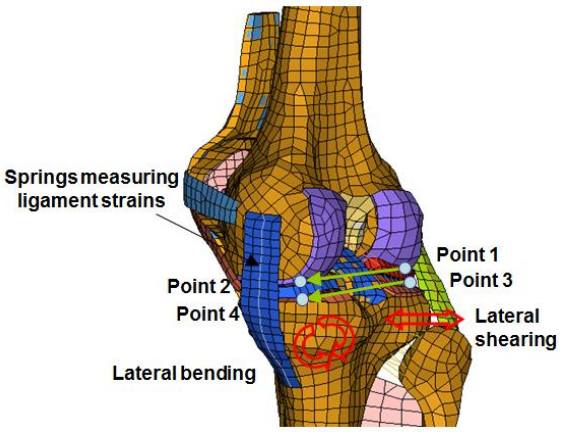

Fig. 2 Measurements of knee ligament strains, lateral bending, and lateral shearing

II. RESULTS

Lower extremity kinematics

As shown in Fig. 3, the node close to the knee joint center height is used as a reference point (zero vertical and horizontal distance). The relative movements of other nodes with respect to this point were measured to reflect lower extremity kinematics. From the time of the initial contact between the pedestrian and vehicle, the responses of lower extremity kinematics measured at each 10 ms are presented in Fig. 3. Although this figure cannot fully reflect the movement in the pedestrian height direction, it respects to the combined effect of lateral bending and shearing.

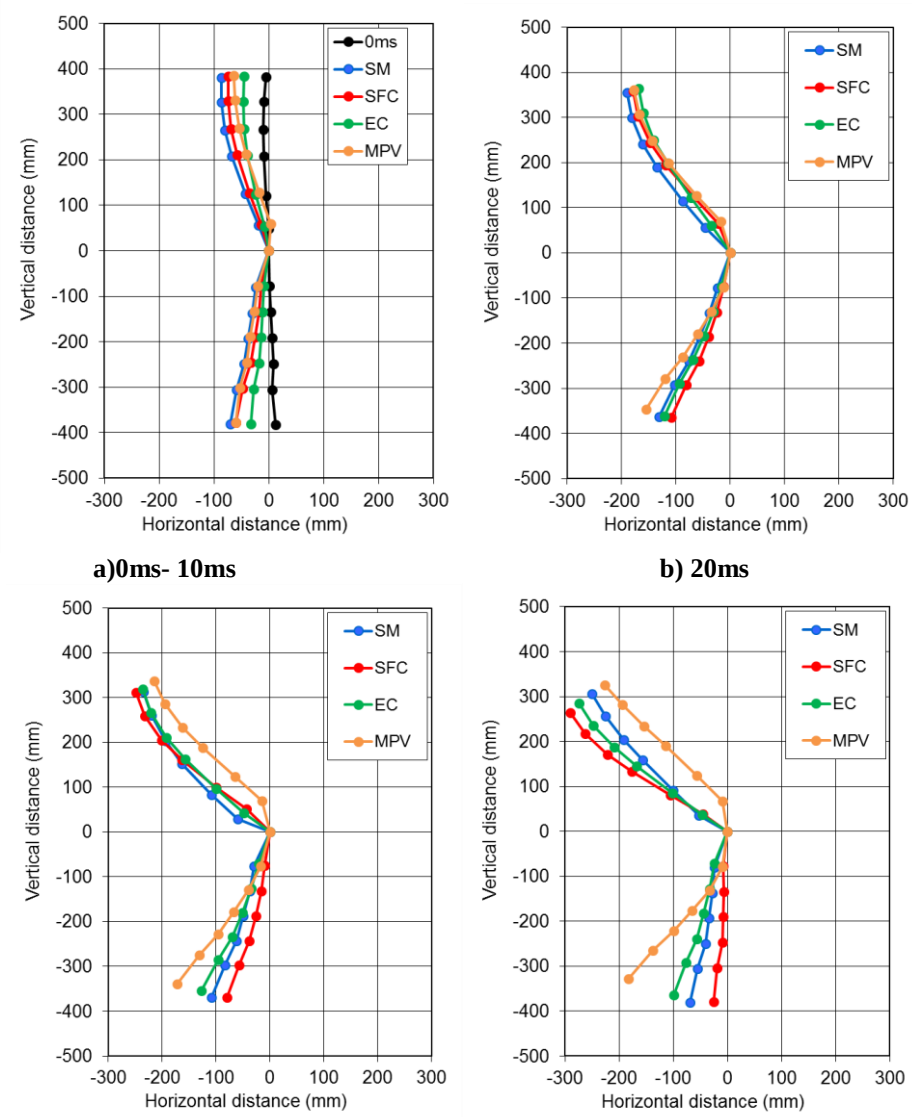

a)0ms- 10ms **b) 20ms**

c)30ms d) 40ms

Fig. 3 Lower extremity kinematics during various vehicle-pedestrian collisions （“Vertical distance” indicates the relative vertical distance of all selected points to the joint center; “Horizontal distance” indicates the horizontal relative distance of all selected points to the joint center）

During the entire impact extent, the lower extremity in collision with the MPV shows a significantly different kinematics if compared with the results obtained with other vehicle models. At 10 ms, the lower extremity presents the smallest bending value in the collision with the EC model. At 20 ms, lower extremity kinematics in all vehicle-pedestrian impacts show similar results. From the movements of the points below or at zero vertical distance (Fig. 3.a,b), the kinematic responses of the tibia show a slight variation from 20 ms to 30 ms in the SM and EC impacts. However, an evident rebound is recorded in the SFC-pedestrian impact. From 30 ms to 40 ms (Fig. 3.c,d), a significant rebound can be noted in the impacts of the SM, SFC, and EC. Apart from the first point below the center height, the other points do not show significant changes in the MPV impact.

On the other hand, the movements of the points above zero vertical distance reflect the kinematic responses of the femur. At 40 ms, the positions of these points show a relation between the lower extremity kinematics and the vehicle front end shapes. The front end shape of these vehicles enlarged gradually from the SFC to the EC, then the SM, finally the MPV (Fig. 1). The kinematic response of the femur follows the same trend at this time (Fig. 3.b).

Tibia fracture risk

Dissecting each instance, the maximum moment of the entire tibia was calculated by comparing moments recorded at different regions. Then a time history can be obtained to find the maximum bending moment during the entire impact simulation. The tibia bending moment vs. time curves of 4 vehicle-pedestrian impacts are shown in Fig. 4a. Corresponding to the time of the maximum bending moment during the impact, the bending moment diagram was acquired to determine various moment distribution along the different tibial regions (Fig. 4b) at the upper recorded value of tibial bending moment.

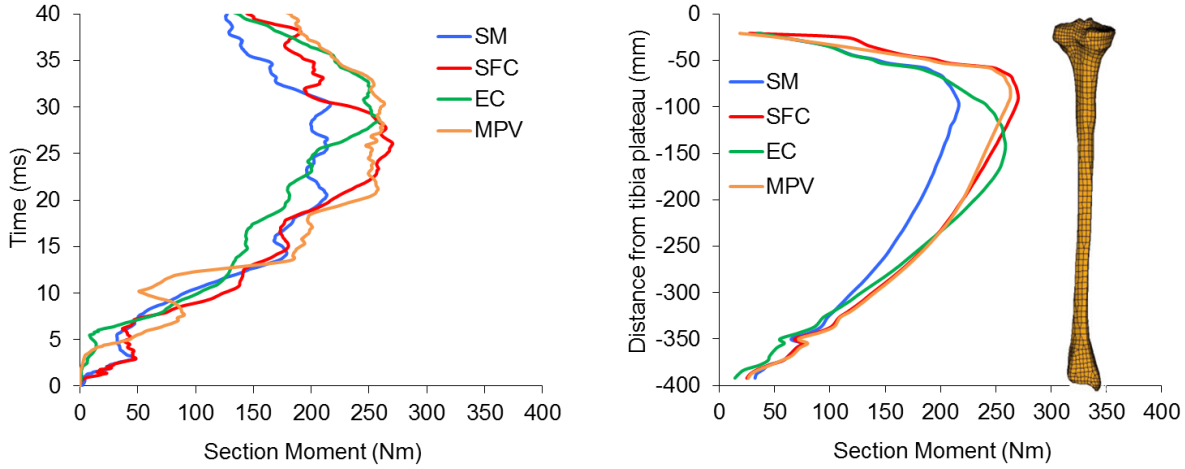

(a) Maximum bending moments to time history

(b) Bending moments of different positions

Fig. 4 Influences of various vehicle front end designs on the tibia bending moment

As shown in Fig. 4a, the SM and the MPV show longer fluctuation at bending moment values close to the peak. The peak value of the tibia bending moment appears early in the collision with the SFC (26.4 ms) than other vehicles. The time for the SM, EC, and MPV are 30.2 ms, 29.4 ms and 28.7 ms, respectively. In Fig. 4b, the tibia bending moment curve shows different features, such as curve shapes of the peaks, peak values, and tibial regions corresponding to the peak values.

Knee ligament rupture risk

For all vehicle-pedestrian impacts, the medial collateral ligaments (MCLs) present the largest deformation compared to other knee ligaments (Fig. 5). The lateral collateral ligaments (LCLs) show the smallest deformation. All ligament strains during the EC-pedestrian impact show extremely different features if compared with others, especially before 12 ms. The strains of both anterior cruciate ligament (ACL) and posterior cruciate ligament (PCL) in the MPV-pedestrian impact show significantly larger peak values between 4 ms and 8 ms (Fig. 5b,c).

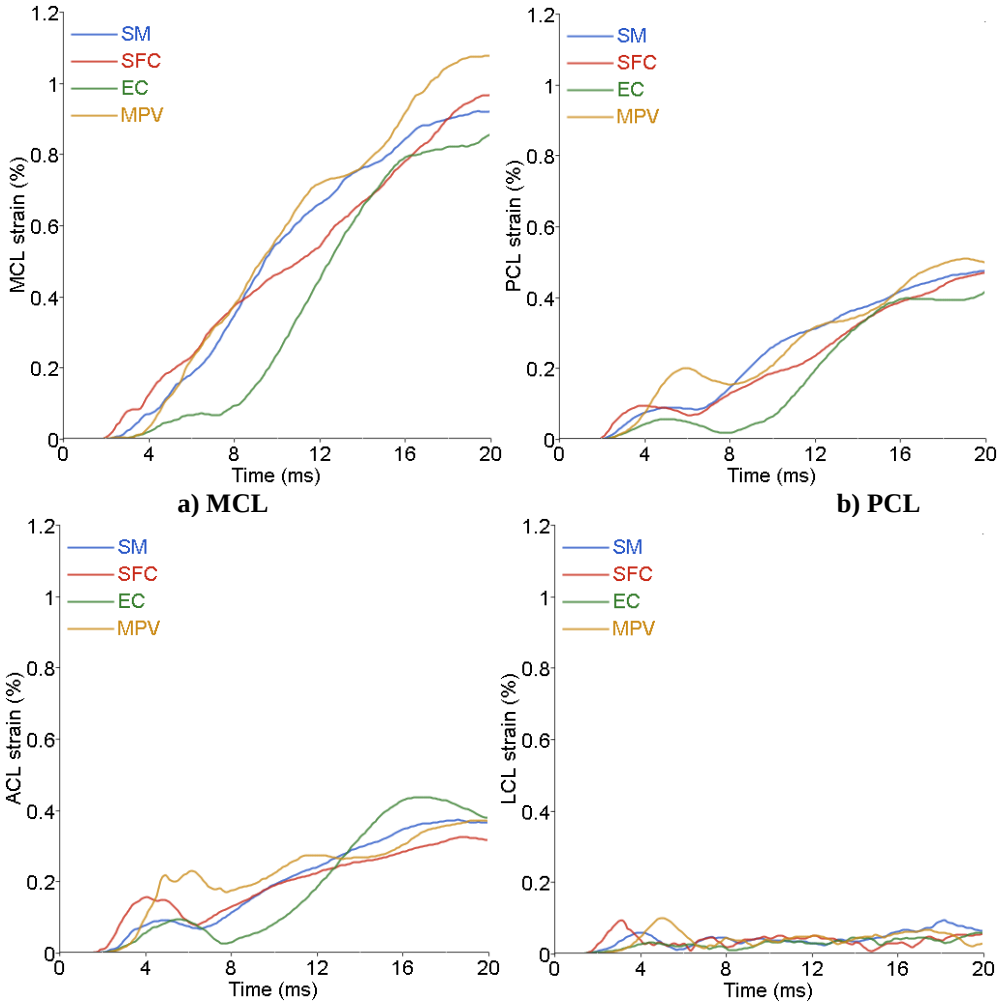

Fig. 5 Influences of various vehicle front end designs on knee ligament strains

Furthermore, the substantial correlation of knee joint kinematics with ligament injuries can be noted by the combination of the Fig. 5 and 6. The trend of the bending curve corresponds well with the trend of the MCL strain variation, as shown in Fig. 5a and 6a. On the other hand, higher absolute shearing values correspond to higher strain values of cruciate ligaments (Fig. 5b,c, and 6b).

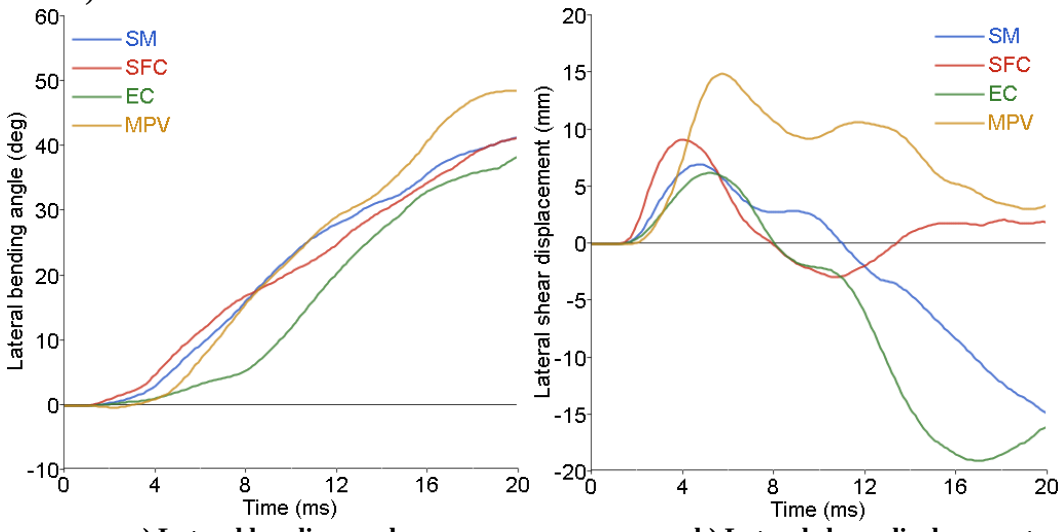

Fig. 6 Influences of various vehicle front end designs on bending and shearing values

III. DISCUSSION

Based on four different vehicle models and a biofidelic lower extremity model, the current study investigated the influences of various vehicle front end designs on the injury risk of the tibia and knee ligaments by finite element simulations. From lower extremity kinematics analysis, differences were obtained by illustrating the various vehicle-pedestrian impact situations (Fig. 3). We noted that when the vehicle bumper gets into contact with the pedestrian, the lower extremity bends around the knee joint following the deformation of the bumper fascia. The bumper beam acts like a non-deformable supporting component, and limits the movement of the lower extremity region that it covers. Thus, both the design of the bumper beam and the shape of the bumper fascia could play an important role in protecting lower extremities of the pedestrian.

As shown in Fig. 3, the lower extremity kinematics of the MPV-pedestrian impact show different features with the impacts of other vehicle types. In fact, we can note in Fig. 1 that the MPV presents a very different front end design compared with other vehicles. Its bumper beam center height (515 mm) is above the knee joint center. All the other vehicles have it below the knee joint center. The bonnet edge of the MPV is also higher than the others. In Fig. 3, the first point above zero vertical distance of the MPV-pedestrian impact keeps close to the zero point in the horizontal direction . If only lateral bending dominates the lower extremity kinematics, the relative distance of these two points would be evident due to the bending effect as noted in other simulation results. So we could postulate that the relative movement of the femur to the tibia from the lateral side of the knee joint to the medial side reduced this relative distance. Fig. 6b also demonstrated this assumption by showing largest shear displacement in the MPV-pedestrian impact. This shear effect could be led by the higher bumper beam of the MPV that mainly covers the region of the femur part. The MPV also shows a larger valgus bending value compared with other passenger vehicle types (Fig. 6a). Again, the higher bumper beam design could be the main reason as it cannot provide enough limits to the bending of lower extremities around the bumper fascia. As we previously described, cruciate ligaments strains increase significantly with lateral shear displacement while the MCL strain with lateral bending. All this could indicate the front end design of the MPV is more aggressive to ligament injuries than other vehicle type designs. The EC impact brings extremely low ligament strain levels, in particular before 12 ms (Fig. 5). From the vehicle design shown in Fig. 1, the EC has a lowest bumper beam and largest space between its bumper beam and bumper fascia. Lower bumper beam would push the lower leg forward, and then limit the total bending of the lower extremity. The larger space between the bumper beam and bumper fascia provides lower stiffness to the front end structure. The combination of these two factors could lead to this phenomenon, and reduce the injury risk of knee ligaments.

In Fig. 5, the MCLs always present the largest deformation as compared to other ligaments. This also proves that the valgus bending dominates all impacts as indicated by the diagram of lower extremity kinematics. By comparing Fig. 5b and c with Fig. 6b, we also noted that high strain levels of cruciate ligaments appear with high shearing values. This phenomenon can be explained as the failure of cruciate ligaments is dominated by lateral shear displacement. These points are in agreement with the findings of Mo et al. (2012). If we consider experimental test results of 18-24% strain for cruciate ligaments and 21%-38% strain for collateral ligaments as injury thresholds (Arnoux et al., 2002), we would postulate that ligaments including the MCL, PCL, and ACL, may all fail during the vehicle-pedestrian impact simulations at 40 km/h. However, the situation presenting all these ligament failures is not often in real accidents. Real vehicle-pedestrian accidents occur in various impact

velocities. The high failure frequency of knee ligaments in our simulations could be due to the high impact velocity in the simulations. The impact velocity of 40 km/h is the current standard test velocity in European pedestrian safety regulation. Thus, our results propose a question if 40 km/h could be too high for testing the protection of vehicle design to the knee ligaments. Hence, the influence of impact velocity on knee ligament injuries should be in depth investigated in the t future by both experimental and simulation methods. In addition, the failure modelling of knee ligaments that were not defined in our model which could also lead to overestimate ligament failures in the simulation. It means we just evaluate the injury risk of knee ligaments by strain values instead of realistically modeling ligament failures in the simulation. Even one ligament fails during the simulation, we keep it intact and continuous to monitor its strain level. Such a method based on strain analysis remains relevant to the time of the first ligament failure. Although it consists of this drawback, it can avoid nonphysical failure occurrence in the simulation and comprehensively evaluate the ligament injury risk.However, due to knee joint kinematics including bending, extension etc., the impact region of the tibia with the bumper beam at rebounding occurrence would be lower than the height of its initial position,nd the impact part of the bumper beam would be also the lower boundary. Other influences of the front end structure could also exist, such as the shape of the bumper fascia and the space between it and the bumper beam etc. Regarding all of these, it could still indicate that the position of the maximum bending moment is related to the lower boundary of the bumper beam. Recent researches also indicated that the tibia tolerance increases gradually from the distal or proximal third to the mid shaft (Mo, Arnoux, Jure,Masson, 2012). Therefore, the lower boundary of the bumper beam could be designed slightly higher than the tibia mid shaft height (200 mm below the knee joint center in the current model) to more efficiently prevent tibia fractures.

In addition, the maximum bending moments in the SFC and MPV impacts give similar values, followed by the EC, then the SM (Fig. 4b). We can note that the SFC and MPV have similar deformable depth between the bumper beam and fascia. The EC presents the largest one (Fig. 1). The SM is the only one without foam component filled between the bumper beam and bumper fascia. This void space leads a softer stiffness compared with the others with a foam component. All these factors could lead the sequence of the maximum bending moment as shown in Fig. 4b. Ivarsson et al. (2005) indicated that the bending moment threshold of the femur mid shaft is 20% higher than the distal third region by considering experimental results. Mo et al. (2012a) also indicated that the tibia tolerance varies with its regions from the proximal third to the distal third by the finite element simulation. Regarding long bone properties, we suppose that the tibia tolerance has a similar situation with the femur. We can reach 280 Nm as the distal third tolerance by scaling the dynamic tolerance of the tibia mid shaft (34 Nm). Taking this tolerance to evaluate the tibia injury by the Fig. 4, we would assume that non tibia diaphysis fractures existed in all impacts. In the current study, only the bumper middle is set as the impact location, which is a region of low stiffness along the horizontal direction of the bumper. Matsui et al. (2011) implemented legform impact tests on different bumper locations of passenger vehicles, and indicated that the side (with components in front of longitudinal beams) part of vehicles would be more aggressive to the pedestrian tibia based on the acceleration level. In the future, we could enlarge our research to investigate tibia fracture risk regarding various impact locations from the side corner of the bumper to its middle. In addition, our discussion in the present study was focused on the front end shape and bumper beam of the vehicle models. Some general influences of these components on pedestrian lower extremity injuries were presented. However, all used car models consist of other different detailed structures, such as the absorber, crash can et al. To extend our understanding on pedestrian lower extremity injuries, the influences of these

structures should be also identified in detail by the future study.

IV. CONCLUSION

The present study investigated the incidences of various vehicle front end structures on lower extremity injuries of pedestrians. Possible ruptures of knee ligaments were examined by total ligaments strains, while tibia fractures by the bending moment. Despite the limitation of the LLMS model, we can investigate the existing relation between these injuries and various front end design of passenger vehicles by comparing lower extremity kinematics with described injury indexes.

We found that the bumper beam design could be a key factor that influences knee ligaments and tibia injuries, such as the bumper beam height, width in the height direction, the deformable depth between it and the bumper fascia. Low bumper beam height could limit joint kinematics and reduce knee ligament injuries. The bending moment distribution of the tibia is related to the bumper height and width, and its maximum value is more or less related to the deformable depth. This indicates that the proper bumper beam height making the peak moment value to appear around the tibia shaft, the wider bumper beam in the height direction, the sufficiently deformable space between the bumper beam and fascia, are all effective actions in designing a vehicle front end to mitigate pedestrian tibia fractures. In the future, this type of research could be continued with a general vehicle front end model to find the correlation between detailed structural design parameters of the vehicle front end and lower extremity injuries.

REFERENCES

1. Mallory A, Stammen J. *Lower Extremity Pedestrian Injury in the U.S.: A Summary of PCDS Data.* NHTSA Vehicle Research and Test Center;2006.

2. Gavrila DM, Marchal P, Meinecke MM. *Vulnerable road user scenario analysis, Deliverable 1-A.* 2003.

3. International Harmonized Research Activities (IHRA). *Pedestrian safety working group 2001 report.* 2001.

4. Cater EL, Neal-Sturgess CE, Hardy RN. APROSYS in-depth database of serious pedestrian and cyclist impacts with vehicles. *Int. J. Crashworthiness.* 2008;13(6):629-642.

5. Arnoux PJ, Cesari D, Behr M, Thollon L, Brunet C. Pedestrian lower limb injury criteria evaluation: a finite element approach. *Traffic Inj. Prev.* 2005 2005;6(3):288-297.

6. Yasuki T. Mechanism analysis of pedestrian knee-bending angle by sedan-type vehicle using human FE model. *Int. J. Crashworthiness.* 2007/10/03 2007;12(4):329-339.

7. Mo F, Arnoux PJ, Jure JJ, Masson C. Injury tolerance of tibia for the car–pedestrian impact. *Accident Analysis & Prevention.* 2012;46(0):18-25.

8. Masson C, Serre T, Cesari D. Pedestrian-vehicle accident: analysis of 4 full scale tests with PMHS. 20th International Technical Conference on the Enhanced Safety of Vehicles Conference (ESV); 2007; Lyon, France.

9. Kerrigan J, Rudd R, Subit D, Untaroiu C, Crandall J, R. R. Pedestrian lower extremity response and injury: A small sedan versus a large sport utility vehicle. SAE 2008 World Congress & Exhibition; 04-14-2008, 2008; Detroit, Michigan, USA.
10. European Experimental Vehicles Committee: Working Group 17 on Pedestrian Proctection. *Improved test methods to evaluate pedestrian protection afforded by passenger cars.* 1998.
11. European Experimental Vehicles Committee: Working Group 10 on Pedestrian Proctection. *Proposals for methods to evaluate pedestrian protection for passenger cars: Final report.* Australia1994.
12. Yasuki T. Mechanism analysis of pedestrian knee-bending angle by SUV type vehicles using human FE model. *Int. J. Crashworthiness.* 2007/12/17 2007;12(6):645-651.
13. Mo F, Masson C, Cesari D, Arnoux PJ. Coupling lateral bending and shearing mechanisms to define knee injury criteria for pedestrian safety. *Traffic Inj. Prev.* 2012;DOI:10.1080/15389588.2012.721146.
14. Martinez L, Compigne S, Guerra LJ. Influence of vehicle shape and stiffness on the pedestrian lower extremity injuries: Review of current pedestrian lower leg test procedure. Paper presented at: 2008 International Research Council on Biomechanics of Injury (IRCOBI) Conference2008; Bern, Switzerland.
15. Committee ECfEIT. Proposal for amendments to global technical regulation No. 9. Geneva2010.
16. Beillas P, Begeman PC, Yang KH, et al. Lower Limb: Advanced FE Model and New Experimental Data. *Stapp Car Crash Journal.* 2001;45(November 2001):469-494.
17. Ivarsson Bj, Kerrigan JR, Lessley DJ, et al. Dynamic response corridors of the human thigh and leg in non-midpoint three-point bending. SAE 2005 World Congress & Exhibition; 2005; Detroit, Michigan,USA.
18. Matsui Y, Hitosugi M, Mizuno K. Severity of vehicle bumper location in vehicle-to-pedestrian impact accidents. *Forensic Sci.Int.* 2011;212(1-3):205-209.